THE KINEMATIC CASCADE AS A HYDROLOGIC MODEL

by

David F. Kibler and David A. Woolhiser

March 1970

HYDROLOGY PAPERS
COLORADO STATE UNIVERSITY
Fort Collins, Colorado

39

THE KINEMATIC CASCADE AS A HYDROLOGIC MODEL

by

David F. Kibler

and

David A. Woolhiser

HYDROLOGY PAPERS
COLORADO STATE UNIVERSITY
FORT COLLINS, COLORADO 80521

March 1970 No. 39

ACKNOWLEDGMENTS

A substantial part of this paper is based upon the Ph.D. dissertation "A Kinematic Overland Flow Model and its Optimization" by David F. Kibler. The work was supported by the Colorado State University Experiment Station and by the Northern Plains Branch, Agricultural Research Service, USDA. Experimental data were obtained from the Colorado State University Experimental Rainfall-Runoff Facility which has been supported in part by grant B-030-COLO by the United States Department of the Interior, Office of Water Resources Research as authorized under the Water Resources Research Act of 1964. The research project also received support from Agricultural Research Service and the Colorado State University Experiment Station under Projects 114 and 124.

TABLE OF CONTENTS

LIST OF FIGURES AND TABLES

ABSTRACT

A kinematic cascade is defined as a sequence of n discrete overland flow planes or channel segments in which the kinematic wave equations are used to describe the unsteady flow. Each plane or channel is characterized by a length, l_k, width, w_k, and a roughness-slope factor, α_k. Outflow from the $k^{\underline{th}}$ plane, along with the parameters for planes k and $k + 1$, establishes the upstream boundary condition for plane $k + 1$. Nondimensional equations are presented for the $k^{\underline{th}}$ element in a kinematic cascade. Properties of the solutions for a kinematic cascade with pulsed lateral inputs are examined. Cascade solutions are compared with characteristic-analytic solutions and with experimental data for flow over a linearly converging section.

THE KINEMATIC CASCADE AS A HYDROLOGIC MODEL*

by

David F. Kibler** and David A. Woolhiser***

Chapter I

INTRODUCTION

Scope and Objectives of the Study

The basic premise underlying the "reductionist" approach to hydrologic modeling is that the complex geometry and topography of natural catchments can be replaced by large numbers of simple elements such as overland flow planes and channels. In its most elementary form, the surface runoff process is thus reduced to the hydraulic problem of unsteady, spatially-varied flow over a uniform plane or channel. The simple plane or channel thus represents a single element in a distributed hydrologic model of the catchment.

In general, a distributed watershed model should possess the following characteristics:

1. The model should be based on sound physical reasoning.

2. The parameters should have direct physical significance.

3. The model should be numerically accurate; i.e., the approximation introduced by finite difference schemes should not influence parameter estimation in any significant way.

4. The model should be subject to experimental verification.

5. The structure of the model should not be so complicated as to require extremely difficult programming logic.

The kinematic cascade is a distributed hydrologic model that exhibits many of these desirable properties and has, therefore, been selected for further analysis in this investigation. The broad objective of this study is to examine certain mathematical properties of the selected model and to describe its application to the problem of watershed transformation and simulation.

The kinematic cascade is defined in this study as a sequence of n discrete overland flow planes or channel segments in which the kinematic wave equations are used to describe the unsteady flow. An n-plane cascade receiving lateral inflow and discharging into a channel segment is shown in Figure 1. Discharge leaving the downstream boundary enters at the upstream boundary of the next plane and establishes the upstream boundary condition for flow on that plane. Discharge leaving the downstream boundary of the last plane is then fed laterally into a channel of known dimensions where it is conveyed via a cascade of channels to some downstream gauging point.

Previous investigators using the kinematic wave technique for simulating watershed response either have relied on severe geometrical simplification or have not examined the approximation errors of their finite difference schemes. Errors caused either by geometric oversimplification or by the finite-difference scheme can affect optimized model parameters in a manner which casts doubt on their physical significance.

Thus, the specific purpose of this study is to evaluate errors introduced by various computational algorithms and by transformation of watershed slope. The dimensionless equations describing kinematic flow over a cascade of planes will first be developed. Solutions to these equations, obtained by the method of characteristics, will then serve as standards in subsequent comparisons with solutions obtained by three rectangular grid methods. The effects of kinematic shock waves, which are produced by exact integration of the characteristic equations for certain cascade configurations, will then be analyzed. A method for tracing the propagation path and a discussion of hydrograph distortions caused by shock propagation are presented. Finally, the effects of transforming the slope of an overland flow surface will be examined by means of outflow hydrograph comparisons. This discussion is prefaced by a brief

* Contribution from the Colorado Agricultural Experiment Station and the Northern Plains Branch, Soil and Water Conservation Research Division, Agricultural Research Service, USDA, Fort Collins, Colorado.

** Associate Engineer, Water Resources Engineers, Incorporated, Walnut Creek, California. Formerly Graduate Student, Colorado State University, Fort Collins.

***Research Hydraulic Engineer, USDA, Fort Collins, Colorado.

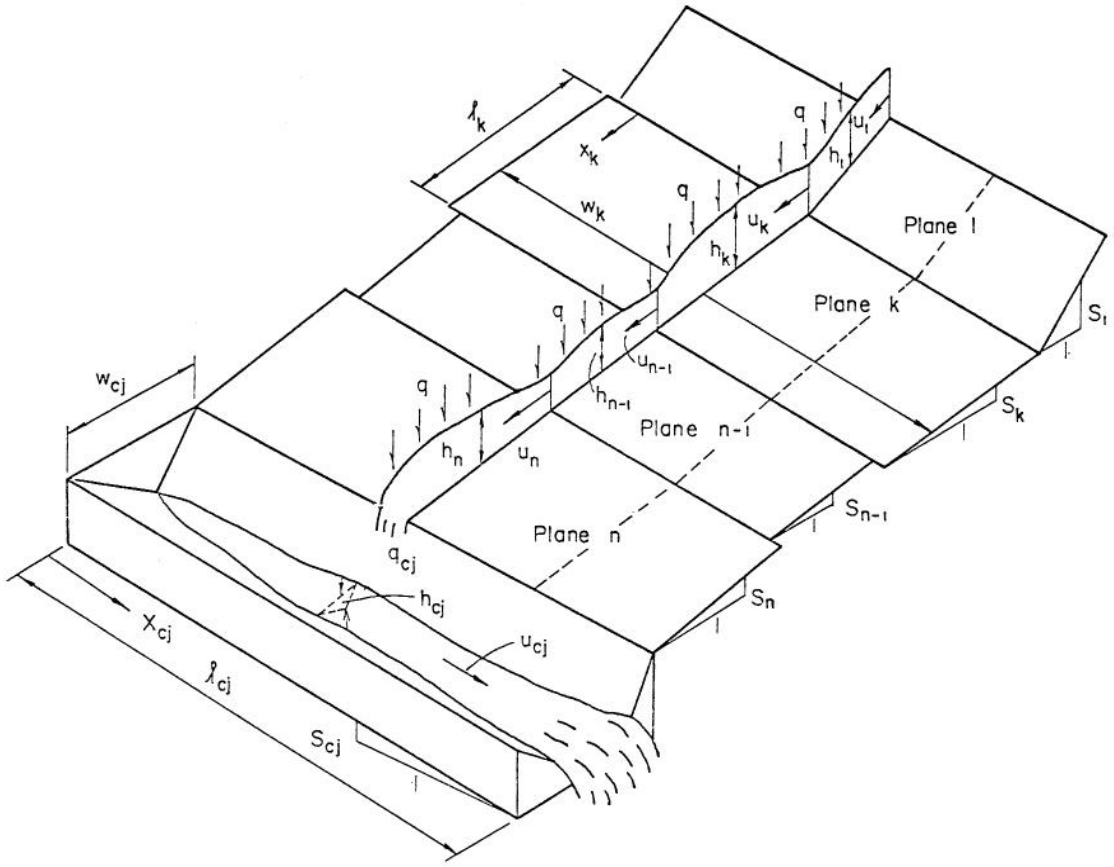

Figure 1. Cascade of n planes discharging into the $j^{\underline{th}}$ channel section.

review of work leading to the formulation of the kinematic cascade as a hydrologic model.

Background of the Kinematic Cascade

The concept of the kinematic cascade was first introduced by Brakensiek (1967a) who transformed an upland watershed into a cascade of planes discharging into a single channel. His transformation technique was based on preservation of the hypsometric curve and the contour length-elevation curve for the watershed. Brakensiek has also written on basic application of the kinematic flood-routing method and has described the properties of the kinematic technique within the context of hydraulic and hydrologic flood-routing procedures (1966, 1967b).

The theory of kinematic flow, which forms the mathematical basis for this hydrologic model, was first set forth by Lighthill and Whitham (1955) in a paper dealing with flood movement in rivers. The authors used the term "kinematic" to describe those waves whose properties are given by the equation of continuity and a stage-discharge relation, such as the Chézy or Manning friction formula. This is in contrast to dynamic or long gravity waves whose motion is governed by both the continuity and momentum or shallow-water equations. Accordingly, kinematic waves possess only one velocity and one system of characteristics along which flow is to be computed. The resulting first-order differential equations for the kinematic wave are in marked contrast to the hyperbolic system associated with the shallow-water equations. The latter possess two families of characteristics and can be solved only by resort to finite-difference methods.

In a paper on the celerity of subsiding flood waves, Henderson (1963) described the conditions under which flow in a prismatic channel (without lateral inflow) could be classified as kinematic. The criterion developed for kinematic flow was that the partial derivative terms appearing in the equation of motion must be negligible in comparison with the bed slope; i.e., the flow must be essentially uniform. It was thus concluded that flood waves will be kinematic in rivers with slopes that are steep, but flatter than those found in torrential mountain streams. Woolhiser and Liggett (1967) also examined the hydraulic conditions required by the kinematic flow assumption and concluded that much of the experimental work on overland flow has been carried out under essentially kinematic conditions.

Iwagaki (1955) used the kinematic assumption implicitly in his analysis of unsteady flow in steep channels. However, the kinematic wave technique was first applied to flow over a sloping plane by Henderson and Wooding (1964). In a series of three papers, Wooding (1965a, 1965b, 1965c) discussed the application of kinematic wave theory to the overland and channel components of runoff from a hypothetical V-shaped watershed consisting of two rectangular planes and a straight channel. Investigation of the response of this elementary watershed system represents one of the first attempts to simulate catchment behavior using the kinematic wave technique.

The rising hydrograph of overland flow on a single plane has been analyzed by Woolhiser and Liggett (1967, op.cit.) using both the shallow-water equations and their kinematic approximation written in dimensionless form. Comparison of results obtained from the complete equations and from the kinematic wave solution disclosed that the degree of departure was related to the dimensionless parameter, k. This parameter is an index representing the magnitude of slope and friction effects--i.e., high values of k indicate that slope and friction dominate the flow and consequently that the kinematic hydrograph is a good approximation to that derived from the complete shallow-water equations. Because of the finding that the shape of the dimensionless hydrograph can be dependent on both k and the Froude number, it was concluded that there can be no unique dimensionless rising hydrograph of overland flow--in contrast to the contention of Izzard (1946). Morgali's (1968) analysis of experimental overland flow hydrographs by means of the kinematic equations is noted in this regard. Woolhiser (1969) has further discussed kinematic flow on an inverted cone-shaped surface having a specified degree of convergence at the apex. This basic watershed element is investigated later in the current study.

The reductionist approach to watershed simulation alluded to earlier in this paper was used by Huggins and Monke (1966) in developing a distributed watershed model. They employed a finite element or square grid technique for decomposing a complex watershed into elemental surface units. The kinematic wave technique was then applied sequentially in the downstream direction to route overland flow generated by each subarea and thereby obtain a complete hydrograph of watershed runoff. As in the kinematic cascade used by Brakensiek, the value of Mannings roughness was adjusted to minimize the discrepancy between observed and computed hydrographs.

Other work on which the present study is based is identified at appropriate points in the text. However, the literature on overland flow is replete with intensive analytical and experimental investigations and clearly, an exhaustive review is outside the scope of the present effort. For a summary of related work in the areas of numerical flood-routing methods, experimental overland flow, mathematical watershed models, and finite-difference solutions to the shallow-water equations reference is made to a publication by Kibler (1968).

Chapter II

KINEMATIC EQUATIONS FOR A CASCADE OF PLANES

The kinematic flow relations are based on the continuity and momentum equations, commonly referred to as the De Saint-Venant or shallow-water equations. These basic equations are derived in Appendix A. In the kinematic wave derivations which follow, the dependent quantities are the local velocity, u, in fps and the depth, h, in feet. The independent variables are the space-time coordinates, x in feet, and t in seconds, respectively.

Kinematic flow on planes and in channels arises whenever a balance between gravitational and frictional forces is achieved. The existence of such a balance implies that the derivatives of the energy and velocity terms in the momentum equation are negligible in comparison with gravity and friction effects. The momentum equation is thus reduced to the form:

$$S = S_f \tag{1}$$

where S and S_f are the bed slope and friction slope, respectively. The hydraulic conditions required by this assumption have been examined by Lighthill and Whitham (op.cit.), Henderson (op.cit.) and by Woolhiser and Liggett (op.cit.).

The continuity equation appears in the usual form for planes or wide rectangular channels

$$\frac{\partial h}{\partial t} + \frac{\partial uh}{\partial x} = q \tag{2}$$

where q is the lateral inflow (precipitation less infiltration) in cfs/ft^2.

In this study a parametric form of the Chézy friction relation is used to represent equation (1) as follows:

$$u = \alpha h^{N-1} \tag{3}$$

where α and N are parameters related to channel (or plane) roughness and geometry. For a wide channel or plane, α and N have values

$$\alpha = C\sqrt{S} \quad ; \quad N = 3/2 \tag{4}$$

where C is the Chézy roughness coefficient.

Dimensionless Equations for $k^{\underline{th}}$ Plane

The characteristic equations can be expressed in dimensionless form by defining normalizing quantities for the $k^{\underline{th}}$ overland flow plane.

Let Q_k = maximum or steady-state discharge per foot of width from the downstream boundary of the $k^{\underline{th}}$ plane resulting from q_k, where q_k is the maximum rate of rainfall excess in cfs/sq.ft. units for the first through the $k^{\underline{th}}$ plane.

$$Q_k = Q_{k-1}\left(\frac{w_{k-1}}{w_k}\right) + q_k\, l_k \tag{5}$$

where l_k and w_k are the length and width, respectively, of the $k^{\underline{th}}$ plane.

In general Q_k is given by the summation

$$Q_k = \frac{1}{w_k} \sum_{i=1}^{k} q_i \cdot l_i \cdot w_i \tag{6}$$

Let L_k = normalizing length for the $k^{\underline{th}}$ plane

$$L_k = \sum_{i=1}^{k} l_i \tag{7}$$

where l_i is the length in feet of plane i.

Let H_k = normal depth in feet corresponding to Q_k at the downstream boundary of the $k^{\underline{th}}$ plane.

$$H_k = \left(\frac{Q_k}{\alpha_k}\right)^{\frac{1}{N}} \tag{8}$$

where α_k and N are Chézy parameters of the $k^{\underline{th}}$ plane.

Let V_k = normal velocity in fps corresponding to Q_k at the downstream boundary of the $k^{\underline{th}}$ plane.

$$V_k = \alpha_k H_k^{N-1} = \alpha_k \left(\frac{Q_k}{\alpha_k}\right)^{\frac{N-1}{N}} \tag{9}$$

Let T_k = normalizing time in seconds for the $k^{\underline{th}}$ plane

$$T_k = \frac{L_k}{V_k} \tag{10}$$

The normalizing quantities have been obtained with the assumption that the planes have equal lengths: $l_1 = l_2 = \ldots = l_n$.

Substituting the parametric friction relation in the continuity equation and using the normalizing quantities of equations (5) through (10), the dimensionless kinematic flow equation for the $k^{\underline{th}}$ plane is given by

$$\frac{\partial h_*}{\partial t_*} + \beta h_*^{N-1} \frac{\partial h_*}{\partial x_*} = q_* \qquad (11)$$

where the asterisk indicates the terms are dimensionless. The only terms in equation (11) previously undefined are q_* and β. The dimensionless lateral inflow is:

$$q_* = \frac{q}{I_k} \qquad (12)$$

where I_k is the normalizing lateral inflow given by

$$I_k = \frac{1}{T_k} \left(\frac{Q_k}{\alpha_k} \right)^{\frac{1}{N}} = \frac{Q_k}{L_k} \qquad (13)$$

and the parameter β is defined as

$$\beta = \frac{\alpha_k N T_k}{\sum_{i=1}^{n} l_i} \left(\frac{Q_k}{\alpha_k} \right)^{\frac{N-1}{N}} = \frac{N L_k}{\sum_{i=1}^{n} l_i} \qquad (14)$$

The dimensionless characteristic equations developed from equation (11) for the $k^{\underline{th}}$ plane in a cascade of n planes are:

$$\frac{dx_*}{dt_*} = \beta h_*^{N-1} \qquad (15)$$

$$\frac{dh_*}{dt_*} = q_* \qquad (16)$$

The asterisk has been dropped from the dimensionless equations for the remainder of this paper except where noted. Integration of equation (16) leads to

$$h = h_o + q(t - t_o) \qquad (17)$$

where h_o and t_o are initial values of depth and time, respectively. The equation of the characteristic curve, obtained by integration of equation (15) is:

$$t = t_o + \frac{1}{q} \left[\left[(x - x_o) \frac{N \cdot q}{\beta} + h_o^N \right]^{\frac{1}{N}} - h_o \right] \qquad (18)$$

When the lateral inflow rate, q, becomes zero, the hydrograph recession is described by the equations:

$$h = h_o \qquad (19)$$

$$x = x_o + \beta h_o^{N-1} (t - t_o) \qquad (20)$$

$$t = t_o + \frac{x - x_o}{\beta} h_o^{1-N} \qquad (21)$$

where x_o, t_o, and h_o are the values of x, t, and h at which the lateral inflow ceases.

The dimensionless velocity of flow on the $k^{\underline{th}}$ plane, as given by the Chézy formula, in terms of the dimensionless depth is:

$$u = h^{N-1} \qquad (22)$$

From equation (22) the dimensionless discharge per foot of width leaving the $k^{\underline{th}}$ plane is obtained as

$$Q = uh = h^N \qquad (23)$$

Equations (17) through (23) can now be used to compute the entire outflow hydrograph arising from known rates of rainfall excess, q, on the $k^{\underline{th}}$ plane.

The problem of hydrograph computation for the $k^{\underline{th}}$ plane is thus completely specified once the initial depths along plane k at time zero and the inflow hydrograph coming from plane $k-1$ are known. The initial and boundary conditions for the cascade are as follows:

$$\text{plane 1:} \quad h_1 (x_1 , 0) = 0$$

$$h_1 (0 , t_1) = 0$$

$$\text{plane k:} \quad h_k (x_k , 0) = 0$$

$$h_k (0 , t_k) = f(h_{k-1} , t_{k-1}) \qquad (24)$$

That is, all planes in the cascade are considered dry at time $t = 0$; the inflow hydrograph coming from the previous plane in the cascade establishes the flow at the upstream boundary for $t > 0$. No flow enters at the upstream boundary of plane 1. Because of the difference in normalizing quantities used in defining the dimensionless flow variables for each plane, it is necessary to convert the depths and times associated with the inflow hydrograph at the upstream boundary to those of the current plane. The following recursion formulas have been developed for that purpose:

$$\frac{t_k}{t_{k-1}} = \frac{k - 1}{k} \left[\frac{w_{k-1}}{w_k} \left(1 + \frac{w_k}{\sum_{i=1}^{k-1} w_i} \right) \right]^{\frac{N-1}{N}} \left(\frac{\alpha_k}{\alpha_{k-1}} \right)^{1/N} \qquad (25)$$

$$\frac{h_k}{h_{k-1}} = \left[\frac{\sum_{i=1}^{k-1} w_i}{\sum_{i=1}^{k} w_i} \right]^{1/N} \qquad (26)$$

where t_{k-1} and h_{k-1} are time and depth at the downstream boundary of plane k-1, and t_k and h_k are the corresponding time and depth at the upstream boundary of plane k . The use of these relationships allows all computations to be done in dimensionless quantities with a general program for plane k.

The dimensionless equations for a cascade of wide rectangular channels are analogous to those for planes and so will not be reproduced here.

Chapter III

KINEMATIC SHOCK-WAVE FORMATION

Several dimensionless rising hydrographs were computed for various two-plane cascades to obtain estimates of the influence of the parameters α (Chézy slope-roughness coefficient) and w (width of plane) on the outflow hydrograph. However, it soon became clear from the hydrograph computations that shock-wave formation occurred for certain α and w combinations and that these shock waves had a profound influence on the properties of the hydrograph. The discussion of this chapter is thus directed at the properties of shock waves in kinematic flow.

A shock wave is represented by the intersections of characteristics in the $x - t$ plane and produces an abrupt increase in flow depth. The surge causes successive wavelets to travel with greater celerity so that earlier wavelets are eventually overtaken and a shock wave, representing the coalescence of wavelets, is formed. Since the discharge-depth relation at the point of intersection of two characteristics is no longer valid, it is necessary to terminate the characteristics at the intersection and fit in the path of the shock. The path of the shock wave in the $x - t$ plane will be given by the locus of the intersection of pairs of characteristics. There are two main objectives in this section: (1) to establish when shock waves will form in terms of the α and w ratios between two successive planes in the cascade; and (2) to devise a technique for tracing the path of a shock wave in the $x - t$ plane and determining the time at which it intersects the downstream boundary of a given plane.

The solution domains are shown for planes k and $k-1$ in Figure 2. The domain enclosed by the line $t = 0$, the downstream boundary and the characteristic originating at $t = 0$ at the upper boundary of the plane is indicated by the letter A. Within this zone the solution depends only on the initial conditions at $t = 0$ for that plane. If the initial conditions are uniform and the overland slope parameters are constant for each plane, characteristics originating along the x-axis at $t_k = 0$ cannot intersect. This is seen from the fact that in order for an intersection to occur, the slopes of the characteristics must bear the following relation at the point of intersection:

$$\left.\frac{dx}{dt}\right|_{\substack{\text{along upper}\\ \text{characteristic}}} > \left.\frac{dx}{dt}\right|_{\substack{\text{along lower}\\ \text{characteristic}}} \qquad (27)$$

Since $\frac{dx}{dt} = \beta h^{N-1}$ and $h = q_k t_k$ in domain A for plane k, the slope $\frac{dt}{dx}$ is constant at any given time t and hence the inequality in equation (27) can never be satisfied in this zone. It follows that a shock can never originate in domain A, although characteristics originating along the upstream boundary may intersect those in domain A. This argument holds for the case of changing q_k, the lateral inflow rate for plane k, since at a given time coordinate q_k will be a known constant and

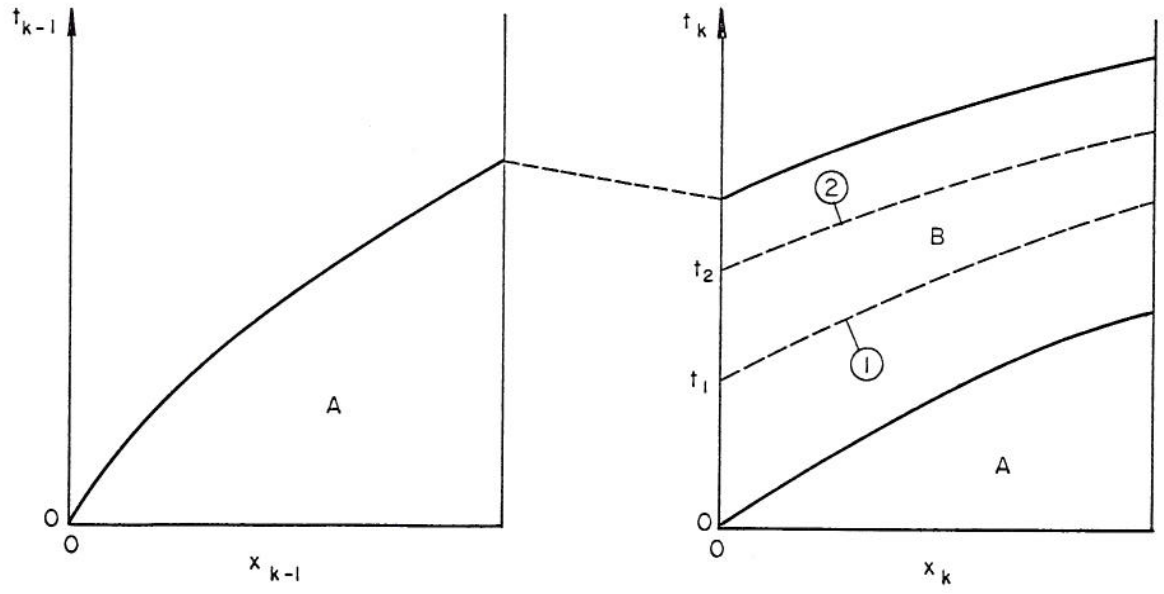

Figure 2. Solution domain for planes k and $k-1$.

hence the slope $\frac{dt}{dx}$ at that point in time is also a constant for all characteristics in A . It is concluded from this argument that a shock wave can never form on the uppermost plane in the cascade for initially dry conditions.

In the domain labeled B in Figure 2, the solution depends upon the upstream boundary condition of plane k which in turn is affected by the initial conditions for plane k - 1 . The necessary condition for an interesection of the characteristics 1 and 2 is:

$$\left.\frac{dx}{dt}\right|_2 > \left.\frac{dx}{dt}\right|_1 \tag{28}$$

where the derivatives are the inverse slopes of the characteristics originating at t_2 and t_1 , respectively. From equations (15) and (25) we obtain the condition at the intersection

$$\beta h_2(x,t)^{N-1} > \beta h_1(x,t)^{N-1}$$

or

$$h_2(x,t) > h_1(x,t) \tag{29}$$

By integrating the characteristic equations we obtain

$$\left.\begin{aligned} h_2(x,t) &= h_2 + q_k(t-t_2) \\ h_1(x,t) &= h_1 + q_k(t-t_1) \end{aligned}\right\} \tag{30}$$

where h_1 , and h_2 are the depths of flow at times t_1 , and t_2 , respectively. Substituting equation (30) into inequality (29) leads to:

$$h_2 - h_1 > q_k(t_2 - t_1) \tag{31}$$

For uniform stepped lateral inflow the depth in zone A for plane k-1 is:

$$h_{k-1} = q_{k-1}\, t_{k-1} \tag{32}$$

By converting t_{k-1} and h_{k-1} to t_k and h_k using equations (25) and (26) and substituting these relationships into inequality (31), we obtain the following after algebraic manipulation:

$$\frac{w_{k-1}}{w_k}\ \frac{\alpha_{k-1}}{\alpha_k} = P_s > 1 \tag{33}$$

Equation (33) defines the shock parameter, P_s , and establishes that shock formation will occur on plane k whenever P_s exceeds unity for the condition of a spatially uniform stepped time-distribution of rainfall excess. Note that while equation (33) is valid for time varying lateral inflow, it does not hold when the inflow changes with distance.

Hence, the inequality of (33) is the general shock-wave criterion, denoted by P_s , for zone B of any plane k . If it is satisfied, then an intersection of any characteristic emanating from the upstream boundary in zone B and a characteristic originating along (x,o) occurs somewhere in the (extended) x - t plane, though not necessarily within the boundaries of the $k^{\underline{th}}$ plane for a sufficiently small interval, $t_2 - t_1$, on the t_k axis. It has been shown that for initially dry conditions and a time-varying, spatially uniform rainfall excess, shock waves cannot originate in zone A of any plane, including plane k = 1 . However, shocks originating in other regions can be propagated into zone A . Further, it is clear that zone B is the critical one from the standpoint of shock-wave formation and propagation in other planes of the cascade. Sequential application of the general rule stated in equation (33) to the k - 2 preceding planes permits one to determine the number of shocks crossing the $k^{\underline{th}}$ plane in the cascade.

Shock-Wave Propagation - Tracing the Shock Path

In an early paper dealing with kinematic flood waves, Lighthill and Whitham (op. cit.) outlined a technique for obtaining the path of a shock wave in the x - t domain. Their semigraphical method is based on continuity of flow and the rate at which flow passes a kinematic wavelet having a given velocity. The procedure described in this chapter is based on the geometry of characteristics which intersect on the shock path and the continuity of flow across the shock front. Figure 3 shows the general features of a shock-wave path as defined by the locus of successive pairs of intersecting characteristics. In particular, two intersecting characteristics, labeled A and B , originate at x_i , t_i , and x_u , t_u , respectively, and carry initial depths h_i and h_u at those points. The space-time coordinates at the point of intersection are x_s and t_s , respectively, as shown for the characteristics labeled A and B in Figure 3.

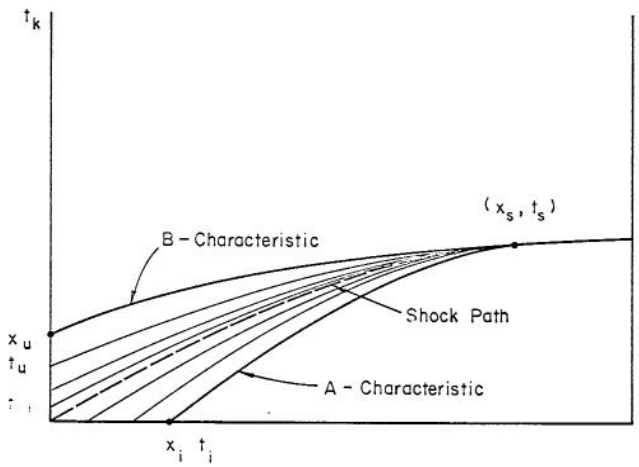

Figure 3. Shock-wave path given by locus of intersecting characteristics.

From the equations for the characteristic ground curves, the following system of equations can be developed for the A and B characteristics:

The B characteristic is defined by:

$$t_b = t_u + \frac{1}{q}\left[\left[(x_b - x_u)\frac{N \cdot q}{\beta} + h_u^N\right]^{1/N} - h_u\right] \qquad (34)$$

where x_b and t_b are coordinates along the B-characteristic curve; N and β are parameters defined previously; q is the rate of lateral inflow; t_u and h_u are the initial values of time and depth, respectively, for the B characteristic.

The A characteristic is defined by:

$$t_a = t_i + \frac{1}{q}\left[\left[(x_a - x_i)\frac{N \cdot q}{\beta} + h_i^N\right]^{1/N} - h_i\right] \qquad (35)$$

Equations (34) and (35) along with an expression for the local velocity of the shock wave

$$V_s = \frac{\beta}{N}\,\frac{h_b^N - h_a^N}{h_b - h_a} \qquad (36)$$

are sufficient to obtain the shock path by a numerical procedure.

Iterative Scheme for Locating the Shock Path

The procedure is as follows. The x axis is divided in increments Δ_s as shown in Figure 4. The shock path originates at the point (0,0) and its velocity is first approximated by expression (36). The time of arrival of the shock at s_2 can then be obtained and equations (34) and (35) can be solved for t_u and x_i. The depths h_b and h_a at s_2 can then be computed and are substituted back into the expression for shock velocity. This iterative procedure is continued until t_2 is stabilized at s_2. Then the shock path is projected to the next coordinate s_3 by using the stabilized flow depths at s_2 in equation (36) and the process is repeated. This procedure is terminated when the downstream boundary is reached. The discharges Q_a and Q_b existing on the shock path at the time of its arrival at the downstream boundary are then inserted in the outflow hydrograph. When all shock paths traversing the $k^{\underline{th}}$ plane have been projected to the downstream boundary, the values of x_i and t_u (or t_i and t_u), corresponding to the intersection at this boundary of each shock path, can be used in filling with characteristics that portion of the x - t plane unaffected by shock-wave propagation. A complete outflow hydrograph, showing the effects of shock formation, can thus be obtained.

Shock-Path Intersections

If a first-order or simple shock wave is defined as the locus of intersecting A and B characteristics, then second-order shocks would be those resulting from the convergence and intersection of adjacent shock paths. While higher order shock waves could conceivably be produced by the mathematical model representing the cascade, attention is focused on the simple or first-order case.

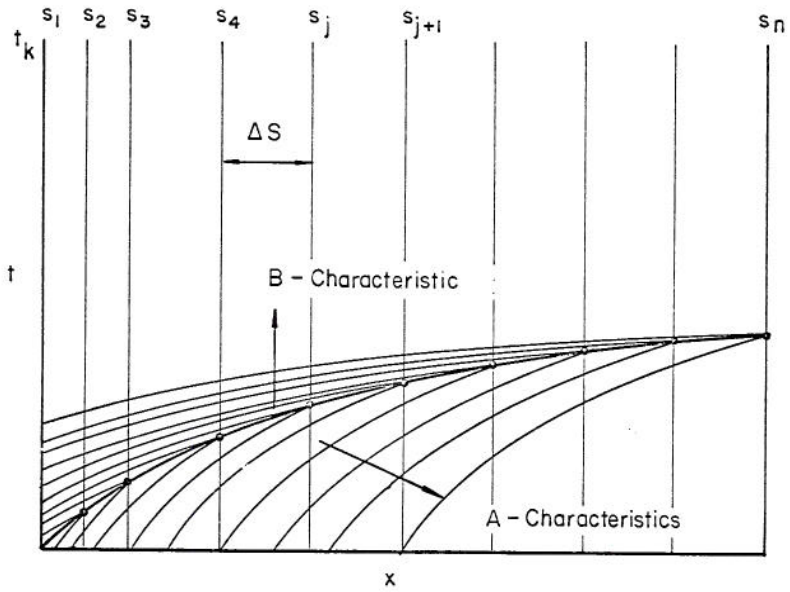

Figure 4. Scheme for describing complete locus of shock-path by use of Δs increments.

Chapter IV

RESULTS OF KINEMATIC SHOCK FORMATION

Tracing the Shock Path

To illustrate certain aspects of the method described in the last chapter, a three-plane kinematic cascade was defined in such a way that shock formation occurred at the origins of planes 2 and 3. The uniform lateral inflow was a pulse of rainfall excess having intensity 0.75 in./hr. and duration 30 minutes. The planes described below are listed in order of highest elevation. All three planes are equal with respect to length, width, and roughness. Only the overland slope is different as indicated by variations in the α parameter.

Table 1. Description of Three-plane Cascade

Plane No.	$\alpha = C\sqrt{S_o}$	Length-ft.	Width-ft.	P_s
1	10.0	400	400	-
2	5.0	400	400	2.0
3	2.5	400	400	2.0

The shock paths crossing planes 2 and 3 are presented in Figure 5. The shock-path computations, involving integrations along the intersecting characteristics, were carried out by means of the dimensionless kinematic flow equations. Only those characteristics which intersect on the shock path at the downstream boundaries of planes 2 and 3 are shown.

Several features of the shock paths presented in Figure 5 are noteworthy. The first is that shock 2-A travels faster than either shock 3-B (a continuation of shock 2-A) or 3-A even though the shock-parameter, P_s, is equal on both planes. This indicates the dependence of absolute shock speed on the overland slope of plane 3, since (assuming constant roughness) the slope of plane 2 is four times that of plane 3. The apparent discontinuity in shock path 2-A is thus attributed to a sudden decrease in velocity upon the shock's arrival at the upstream boundary of plane 3.

Another interesting aspect of the shock paths illustrated in Figure 5 is the constant velocity of propagation achieved over the lower portions of each plane. This can be observed from the linearity of shock 3-B over the entire length of plane 3. Such a

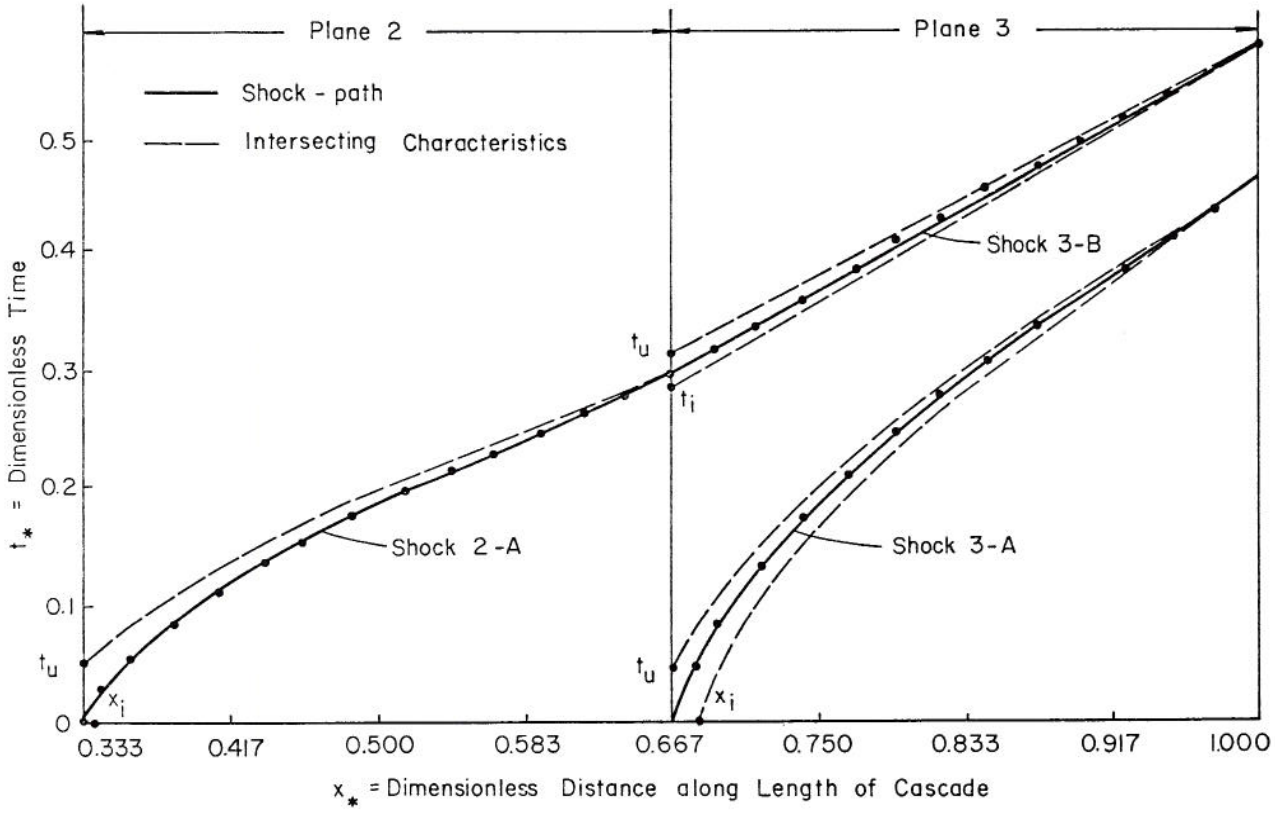

Figure 5. Shock-paths on planes 2 and 3 for the cascade of Table 1.

condition, once detected, could be used to project the shock path across greater distances and thereby increase the speed of the iterative procedure described in the last section.

The outflow hydrograph for plane 3, showing the surges in discharge associated with shocks 3-A and 3-B, is presented in Figure 6. The outflow hydrograph obtained when shocks 3-A and 3-B are ignored is shown for purposes of comparison by means of a dashed line in Figure 6. This hydrograph was obtained by eliminating from the computations those characteristics passing through disturbed regions of the $x_* - t_*$ plane created by the shock. It therefore represents an approximate solution over the two intervals, shown in Figure 6, which are affected by the arrival of kinematic shock waves.

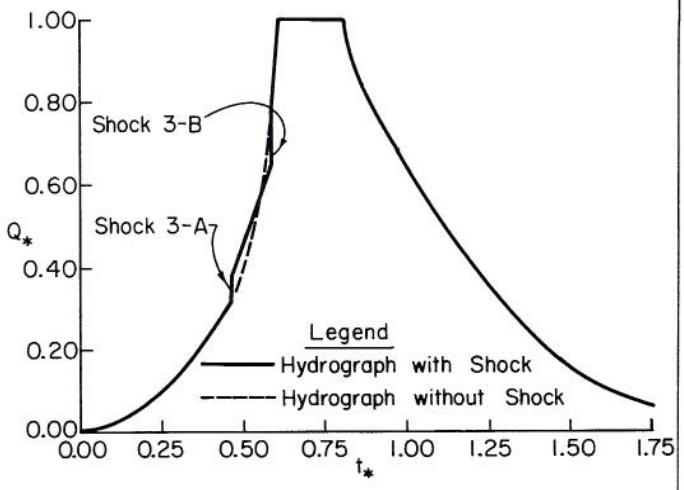

Figure 6. Dimensionless hydrograph for cascade of Table 1 showing effect of 2 shocks on plane 3.

Shock Paths for Various 2-plane Cascades

In order to examine the effect of the shock parameter, P_s, on the shock path, a number of 2-plane cascades were defined as indicated in Table 2. The lengths and widths of the upper planes were held constant while the slopes, as represented by the α parameter, were varied between the limits: $1.25 < \alpha < 10.0$. The lower plane was maintained at a constant length, width and slope for all cascades. The Chézy C factor was assumed constant for all planes. The resulting ratios of overland slopes for the upper and lower planes in each cascade are also listed in Table 2. Lateral inflow was given as a uniform pulse having intensity 0.75 in./hr. and duration 30 minutes.

The family of shock paths observed on plane 2 of the cascades described in Table 2 is presented in Figure 7. The influence of the shock parameter, P_s, is clearly evident from the decreasing passage times of shocks associated with high P_s values. This result indicates the dependence of shock velocity on P_s when the slope of the lower plane is held constant.

The same shocks would occur if the slopes for each plane were the same but if the Chézy C were varied so that α remained as shown in Table 2.

Table 2. Description of upper and lower planes in 2-plane cascades.

Cascade No.	α-slope	Length ft.	Width ft.	P_s	S_1/S_2
(upper planes)					
1	1.25	100	400	1.25	1.56
2	1.50	100	400	1.50	2.25
3	1.75	100	400	1.75	3.06
4	2.00	100	400	2.00	4.00
5	2.50	100	400	2.50	6.25
6	3.00	100	400	3.00	9.00
7	4.00	100	400	4.00	16.00
8	5.00	100	400	5.00	25.00
9	6.00	100	400	6.00	36.00
10	7.00	100	400	7.00	49.00
11	8.00	100	400	8.00	64.00
12	9.00	100	400	9.00	81.00
13	10.00	100	400	10.00	100.00
(lower planes)	1.00	100	400	-	-

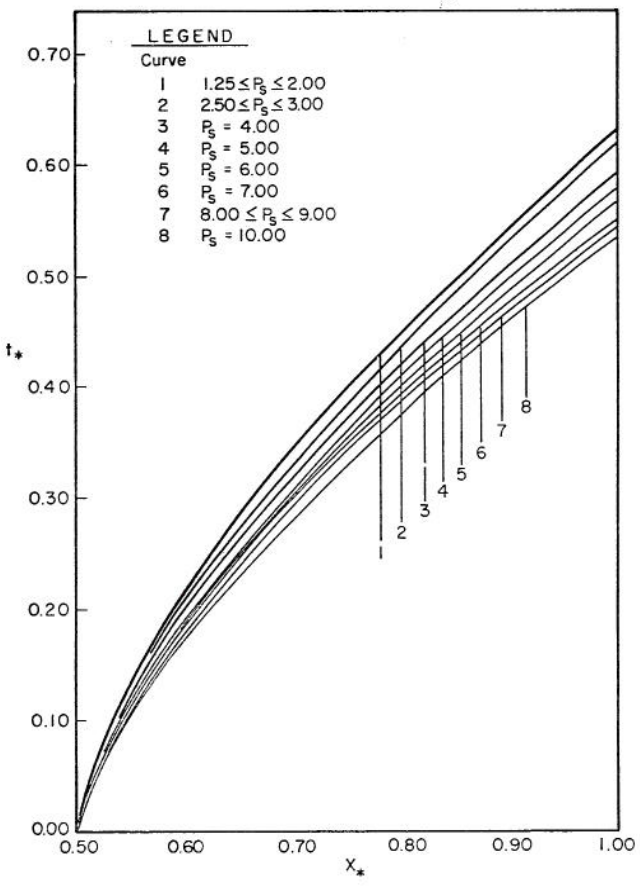

Figure 7. Shock-paths in dimensionless $x_* - t_*$ plane for various P_s values and cascades of Table 2.

In order to more fully investigate the effect of changing P_s on the shock path, another series of 2-plane cascades was defined. According to this definition, the upper plane was held constant with $\alpha = 10.0$, length = 400 feet, and width = 400 feet. The lengths and widths of each lower plane were set at 400 feet, while the overland slope was varied in the range $1.00 < \alpha < 8.00$. The shock parameter was thus given values over the interval $1.25 < P_s < 10.00$ as in the previous set of cascades.

The resulting shock paths possessed the general features presented in Figure 7, except that they varied with P_s in reverse order. That is, the shock paths associated with higher values of P_s arrived at the downstream boundary of plane 2 later than those having a smaller value of P_s. This inverted relation between P_s and time of arrival is a result of the shock traveling across an overland plane of small slope compared with the second plane having the same P_s in the previous set of cascades described in Table 2.

Outflow Hydrographs for Various 2-plane Cascades

The outflow hydrographs observed at the downstream boundary of the second plane for the cascades of Table 2 are presented in Figure 8. It is observed that the hydrographs for all cascades coincide over the regions that are outside the influence of the shock front. The effect of P_s is evident from the varying position of the vertical portion of the rising limb representing the surge in flow created by shock formation. Previous results have shown that both the strength and velocity of the shock will increase directly as P_s for the cascades of Table 2. This relationship is clearly observable in the outflow hydrographs of Figure 8.

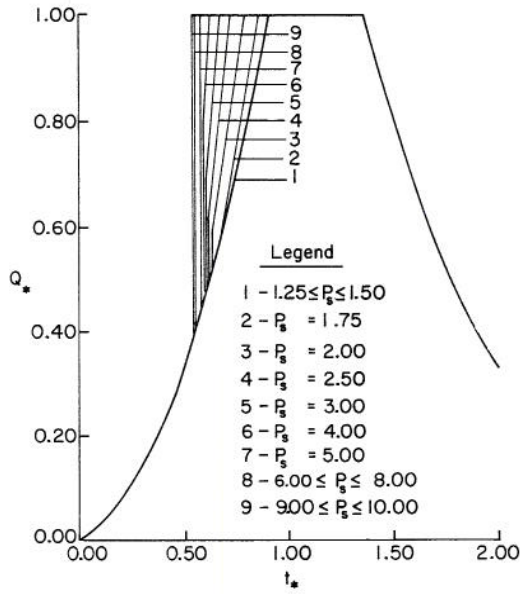

Figure 8. Dimensionless outflow hydrographs for various P_s values and cascades of Table 2.

The dimensionless shock paths and rising hydrographs presented in Figures 7 and 8, respectively, are perfectly general for cascades of 2 planes, having equal lengths, widths, and roughness, in which the lower plane is fixed with respect to overland slope. The equilibrium and recession portions will vary according to the equilibrium time of the lower plane, which in turn is a function of the length, width, and slope of both planes. Since the discussion of this section has centered on the effect of shocks on the rising limb, further dimensionless results are not presented.

Kinematic Shocks in Partial Equilibrium Hydrographs

When lateral inflow ceases before steady-state conditions are established, outflow from the lower plane peaks at a rate less than that of the lateral inflow pulse. Because characteristics become straight lines and carry constant depths after lateral inflow ceases, it is anticipated that the depths across the shock and consequently the shock path itself will differ from the full equilibrium case.

In order to determine the effect of shock formation on partial equilibrium hydrographs, the 3-plane cascade of Table 1 was run for a lateral inflow pulse of intensity 0.75 in./hr. and durations 15, 20 and 25 minutes. Since the 3-plane cascade reaches equilibrium in approximately 22 minutes for this lateral inflow rate, the first two cases will produce partial equilibrium hydrographs while the third will produce full equilibrium.

The resulting 3-plane hydrographs are shown in Figure 9 in which shocks A and B are indicated by heavy vertical lines. Several features of Figure 9 are of interest. The first is that, although the depths across shocks A and B decrease with decreasing pulse length, the speed of each shock remains approximately constant. Hence the shock path is not significantly affected by cessation of lateral inflow.

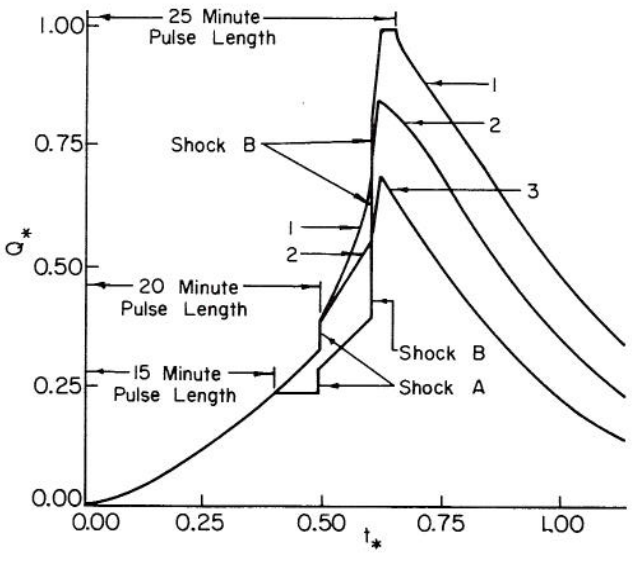

Figure 9. Dimensionless partial equilibrium hydrographs for the 3-plane cascade of Table 1 with 2 shocks on plane 3.

A simple computation reveals that the shock strength, as measured by the ratio h_B/h_A, is roughly constant for shock A and shock B occurring in the hydrograph of Figure 9. This result is in agreement with the motion of a shock wave whose speed is independent of lateral inflow cessation.

Another interesting aspect of Figure 9 is that portion of the hydrograph which connects the two shocks. It is evident that this connecting portion becomes flatter as the pulse duration is decreased. If the pattern observed in hydrograph 3 were continued, it is expected that eventually the linkage between successive shocks would become horizontal. The resulting partial equilibrium hydrograph would then exhibit a stair-step structure in the region affected by the arrival of successive shock waves. This feature, observed in hydrograph 3, is a consequence of shocks arriving at the downstream boundary after lateral inflow has stopped.

Iwagaki (1955) performed some laboratory experiments involving unsteady, open-channel flow with lateral inflow. One set of experiments was run in a flume 24 meters long, where the uppermost 8-meter section had a slope of 0.020, the middle section slope was 0.015 and the lower section slope was 0.010. Under conditions of uniform lateral inflow the kinematic model would predict three shocks. Iwagaki, however, adjusted the lateral inflow supply so that the middle section had a lower rate of lateral inflow than the upper and lower section. The hydrographs he obtained are reproduced in Figure 10. These hydrographs can be qualitatively compared with the partial equilibrium hydrographs in Figure 9. Obviously the physical manifestation of a kinematic shock is a rapid rise in the outflow rate as the shock reaches the downstream boundary. Furthermore, it appears that the kinematic representation of a shock will lead to errors in a very small region of the outflow hydrograph.

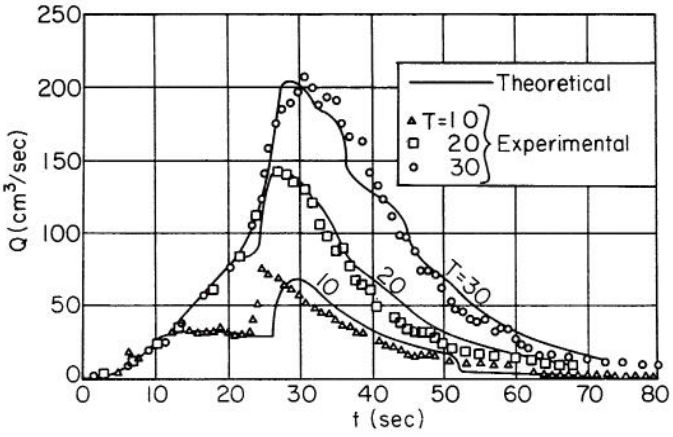

Figure 10. Theoretical and experimental overland flow hydrographs showing physical manifestation of kinematic shock waves (after Iwagaki, 1955).

Difference Solutions to the Kinematic Equation Using Rectangular Grids

In investigating the properties of the kinematic cascade it seemed desirable to use the method of characteristics and a characteristic net to minimize errors. The possibility of large discontinuities in the solution at kinematic shock waves also seemed an important consideration in the choice of a numerical method. For practical cases, however, rectangular grid schemes are much easier to work with. Accordingly, we compared solutions from three rectangular grid schemes with solutions obtained by the method of characteristics. The three rectangular grid methods used were: (1) the upstream differencing method; (2) the single-step Lax-Wendroff scheme (Houghton and Kasahara, 1968) and (3) the four-point implicit scheme used by Brakensiek (1967a). The finite difference formulation, the order of approximation and the linear stability criterion for each of these schemes is shown in Table 3. The derivation of the single-step Lax-Wendroff method and stability calculations for the three methods are included in the Appendix. For a definition sketch of the notation in Table 3, see Figure 11.

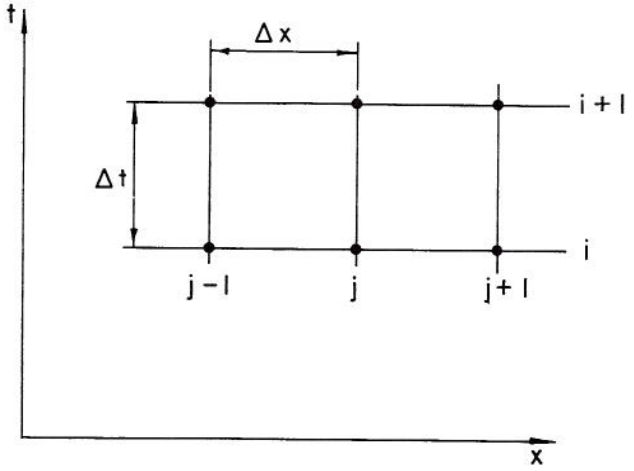

Figure 11. Notation for finite-difference schemes.

Dimensionless hydrographs computed by the above three methods and by the method of characteristics are shown in Figure 12. The input pulse duration was equal to the time to equilibrium of the 2-plane cascade. The smoothing effect of the rectangular schemes is clearly shown and the second-order Lax-Wendroff method does give the best approximation. In general, the peak response is delayed and reduced by as much as 20% for the first-order schemes. Differences of this magnitude seem to be sufficiently great to warrant further examination.

We have not experienced any instabilities in the difference schemes attributable to the shocks, but this is a possibility. In Brakensiek's method the equation for h_j^{i+1} is nonlinear and must be solved by an iterative procedure. With strong shocks and small Δt increments there was no positive solution for this equation for the first Δx increment on the second plane. However, Brakensiek's method has the important advantage of unconditional stability which may result in more rapid calculations because fewer steps are required. This advantage may be partially or completely offset by the iterative procedure required.

Table 3. Rectangular Grid Finite-Difference Schemes

Method	Finite Difference Equation	Order of Approximation	Linear Stability Criterion
Single-Step Lax-Wendroff	$h_j^{i+1} = h_j^i - \Delta t \frac{k}{n}\left[\frac{\left(h_{j+1}^{iN} - h_{j-1}^{iN}\right)}{2\Delta x} - \frac{1}{2}\left(q_{j+1}^i + q_{j-1}^i\right)\right] + \frac{\Delta t^2 Nk}{4n\Delta x}\left\{\left(h_{j+1}^{iN-1} + h_j^{iN-1}\right)\left[\frac{k}{n}\frac{\left(h_{j+1}^{iN} - h_j^{iN}\right)}{\Delta x} - \frac{1}{2}\left(q_{j+1}^i + q_j^i\right)\right] - \left(h_j^{iN-1} + h_{j-1}^{iN-1}\right)\left[\frac{k}{n}\frac{\left(h_j^{iN} - h_{j-1}^{iN}\right)}{\Delta x} - \frac{1}{2}\left(q_j^i + q_{j-1}^i\right)\right] + \frac{2n\Delta x}{Nk\Delta t}\left(q_j^{i+1} - q_j^i\right)\right\}$	$0(\Delta x)^2$	$\frac{\Delta t}{\Delta x} \le \frac{n}{Nk\bar{h}^{N-1}}$
Upstream Differencing	$h_j^{i+1} = h_j^i - \frac{Nk}{n}\frac{\Delta t}{\Delta x}\left(h_j^{iN} - h_{j-1}^{iN}\right) + q_j^i \Delta t$	$0(\Delta x)$	$\frac{\Delta t}{\Delta x} \le \frac{n}{2.75kNh^{N-1}}$
Brakensiek's Four Point Implicit	$\frac{h_j^{i+1} - h_j^i + h_{j-1}^{i+1} - h_{j-1}^i}{2\Delta t} + \frac{k}{n\Delta x}\left(h_j^{i+1N} - h_{j-1}^{i+1N}\right) - \frac{1}{4}\left(q_{j-1}^{i+1} + q_j^{i+1} + q_{j-1}^i + q_j^i\right) = 0$	$0(\Delta x)$	Unconditionally stable

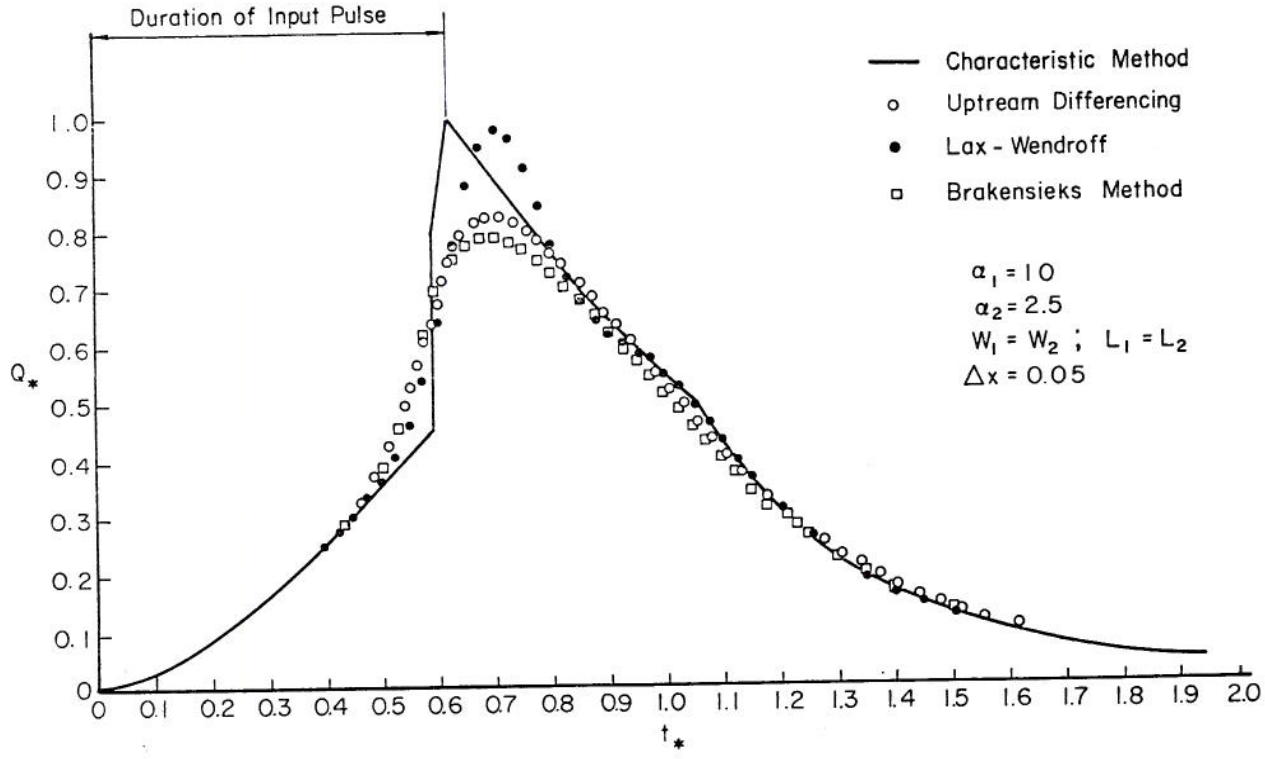

Figure 12. Comparison of finite-difference methods.

Chapter V

APPLICATIONS OF THE KINEMATIC CASCADE TO COMPLEX WATERSHED GEOMETRIES

In any practical application, use of the kinematic cascade to simulate surface runoff from complex watersheds will introduce certain errors of approximation. These errors are associated with the manner in which the cascade is adapted to actual watershed configuration. For example, a converging overland surface will be replaced by a series of rectangular planes with decreasing widths, while a complex continuous overland slope will be represented by a series of discrete planes with individually uniform slopes. It is evident that by making the individual plane lengths small enough (i.e., increasing the number of planes in the cascade) we can minimize the errors of approximation associated with the kinematic cascade transformation.

Comparison with Exact Solutions for a Converging Surface

One test of the kinematic cascade is to determine how well cascade solutions conform to those exact solutions obtained for selected watershed shapes. Woolhiser (1969) has obtained such exact solutions for kinematic flow on a converging surface, as shown in Figure 13. The purpose of this chapter is to compare kinematic cascade solutions with kinematic solutions for overland flow on a converging watershed surface.

For the geometry of the converging section shown in Figure 13, the continuity equation has been written by Veal (1966) as:

$$\frac{\partial h}{\partial t} + \frac{\partial uh}{\partial x} = q + \frac{uh}{(L_o - x)} \qquad (37)$$

The momentum equation is given by the friction relation of equation (3). Woolhiser (1969) has derived the characteristic equation, based on equations (3) and (37), and has put them in dimensionless form. He introduced a parameter r which defines the degree of convergence exhibited by the section--a small value of r indicates high flow convergence, while as r approaches unity, the convergence of flow tends toward that of a plane rectangular surface.

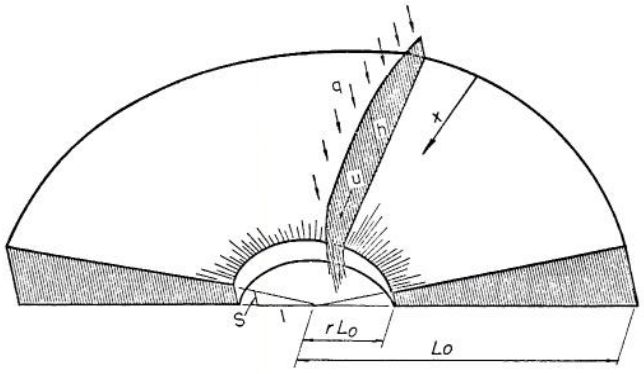

Figure 13. Geometry of converging section.

The test case selected had the following parameters:

$L_0 = 100$ ft.; $r = 0.1$; Chézy $C = 100$;

$S = 0.05$; $N = 3/2$

The rainfall excess was 1 in./hr. applied for 90 seconds.

In approximating the above converging section with a kinematic cascade we have a choice of the total number of planes, defined by n , and the size of the Δx increment for rectangular grid schemes. The total number of grid points in the x-direction is $1/\Delta x + 1$. Hydrographs were computed for cascade configurations ranging from one plane to ten planes of equal length, with a maximum of 21 grid points in the x direction. The width of the $i^{\underline{th}}$ plane of an n-plane cascade was calculated by the following area-preserving relation

$$w_i = \frac{\theta r L_0}{360} \cdot \left[2 + \left(\frac{1-r}{n}\right)\left(1-2i\right) \right] \qquad (38)$$

$$i = 1, 2 - - - n$$

where θ is the angle subtended by the converging section.

Hydrograph calculations were carried out by using the second-order Lax-Wendroff scheme for the interior of each plane, while the upstream differencing method was used at the downstream boundary. The results of these computations are shown in Figures 14(a), (b), (c), and (d). The parameter B in Figure 14 is equal to the number of Δx increments in each plane. Therefore, nB is the number of increments in the cascade and is related to the number of computations performed. The information in Figure 14 is summarized in Figure 15 where an error index is shown as a function of nB , with n as a parameter. The error index is defined as the sum of the difference between the characteristic-analytic solution and the finite difference solution at the time to equilibrium and at the time that lateral inflow ceases. This is admittedly a rather crude index and it is not recommended for general use. However, it is adequate for this special case.

An examination of Figures 14 and 15 shows that the error index decreases as nB increases for any n , but that very little accuracy is gained by increasing nB from 15 to 20. The error index decreases as n goes from 1 to 3, but for this case there appears to be a decrease in accuracy as n is increased from 3 to 4. This probably occurs because as the number of planes is increased, the first-order differencing scheme for the lower boundary is used

more frequently and eventually decreases the overall accuracy of this solution. Shocks present in the cascade solutions have been smoothed by the finite-differending method used to obtain outflow hydrographs. Although this is by no means an exhaustive test, it appears that the kinematic cascade is very effective in handling lateral convergence and that three planes with Δx increments of 0.0667 L_o will give satisfactory results for linearly converging flow with r = 0.10.

Effect of Changing Overland Slope on Cascade Hydrographs

A second set of computations was performed to examine the effect of varying overland slopes on hydrograph shape. The slopes of each 3-plane cascade are shown in Table 4.

Table 4. Cascade Slopes

Run No.	Slope of Plane		
	S_1	S_2	S_3
1	.0197	.05	.08
2	.08	.05	.0197
3	.025	.10	.025
4	.065	.02	.065
5	.05	.05	.05

Each plane of the 3-plane cascades was 36.67 ft. long, 1 foot wide, and has a Chézy coefficient C = 100. The total relief for each cascade was 5.5 ft. A rainfall excess of 1.00 in./hr. was applied for 100 seconds which is the time of equilibrium of a single plane 110 ft. long with 5 percent slope.

The results of the computations are shown in Figure 16. The general shape of the rising hydrograph is the same as the shape of the overland slope. The time to peak is not greatly affected by the shape of the overland-slope profile for this near-equilibrium situation, but it would be significantly affected for partial equilibrium cases. There is a maximum difference of 10 percent in the peak rates, with the constant slope cascade having the highest peak and the complex slopes (runs 3 and 4) having the lowest peak rate. The Lax-Wendroff scheme was used for all computations, so the same type of errors as evidenced in Figure 11 are present. Shocks should theoretically occur in cases 2, 3, and 4. The finite-difference scheme smooths these shocks and probably attenuates the peaks. It is apparent from this example that, for surfaces with the same length and relief, shape of the overland-slope profile is a significant factor in determining the shape of the rising hydrograph of outflow from the kinematic cascade.

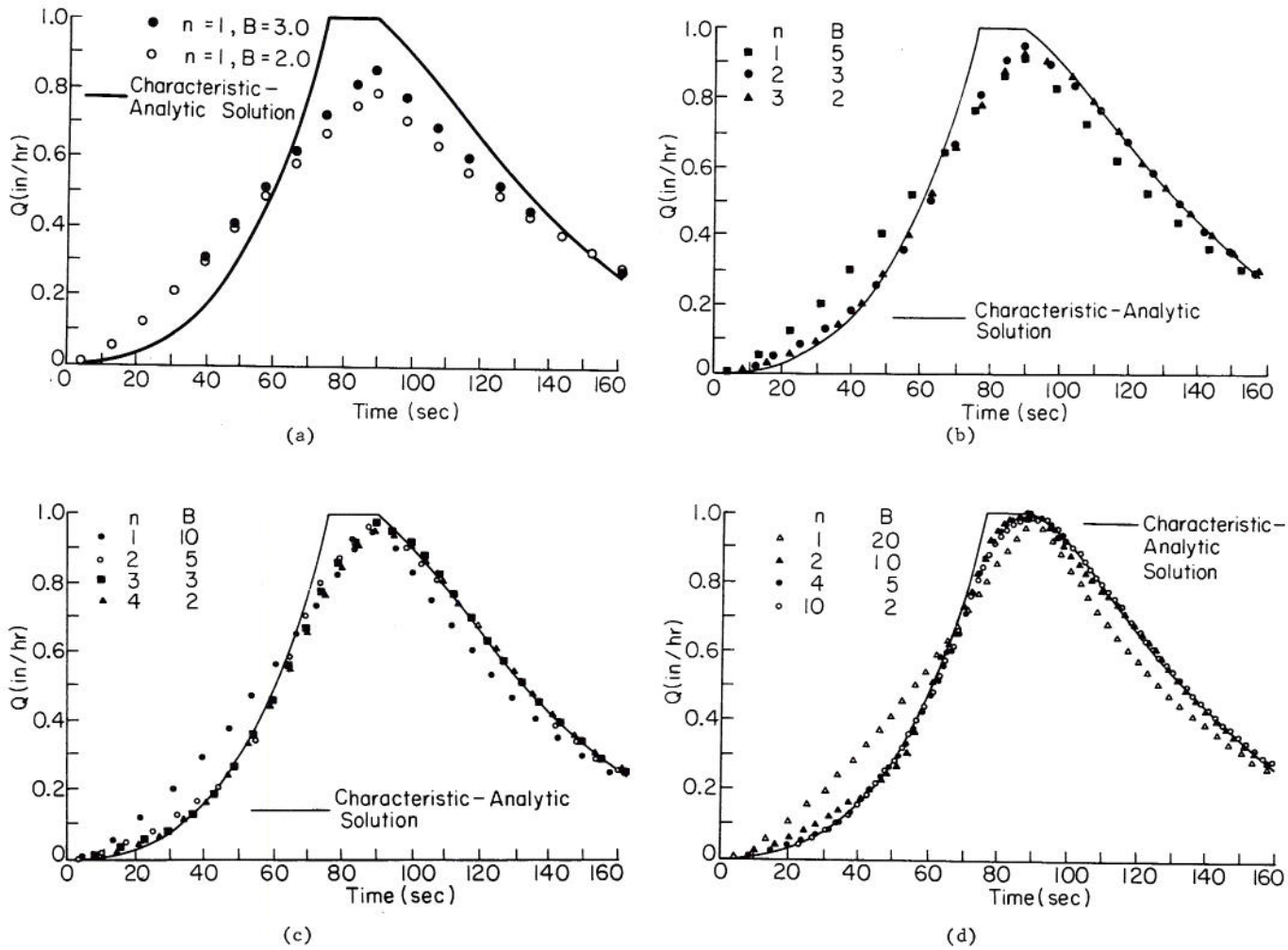

Figure 14. Kinematic cascade results compared with characteristic-analytic solution converging section r = 0.10 L_o = 100

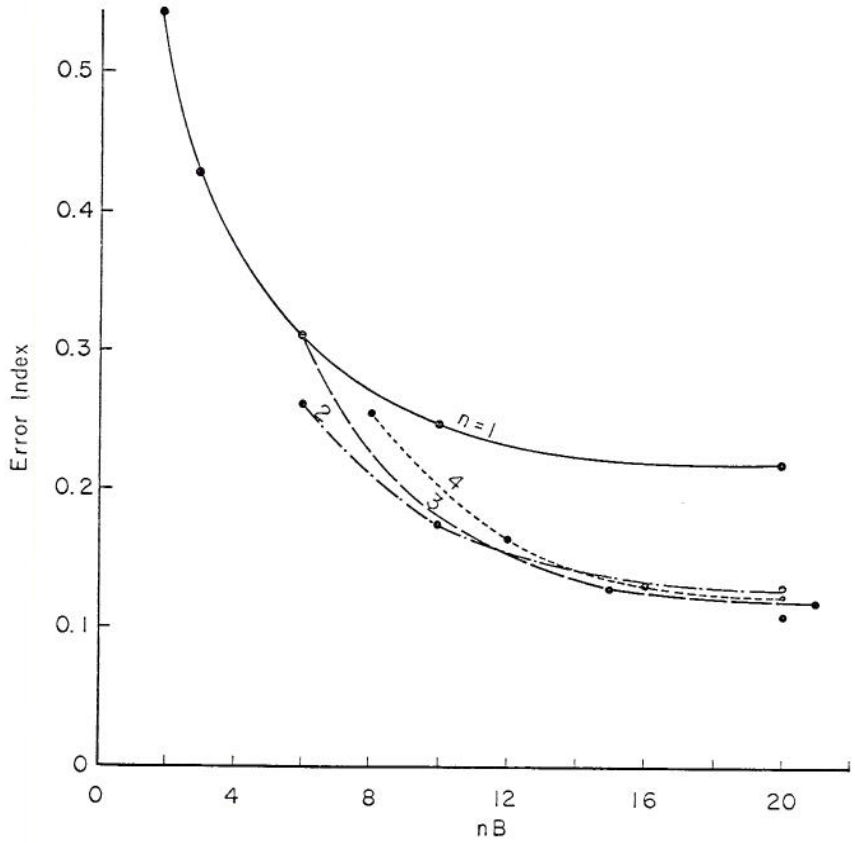

Figure 15. Effect of number of Δx increments on error index.

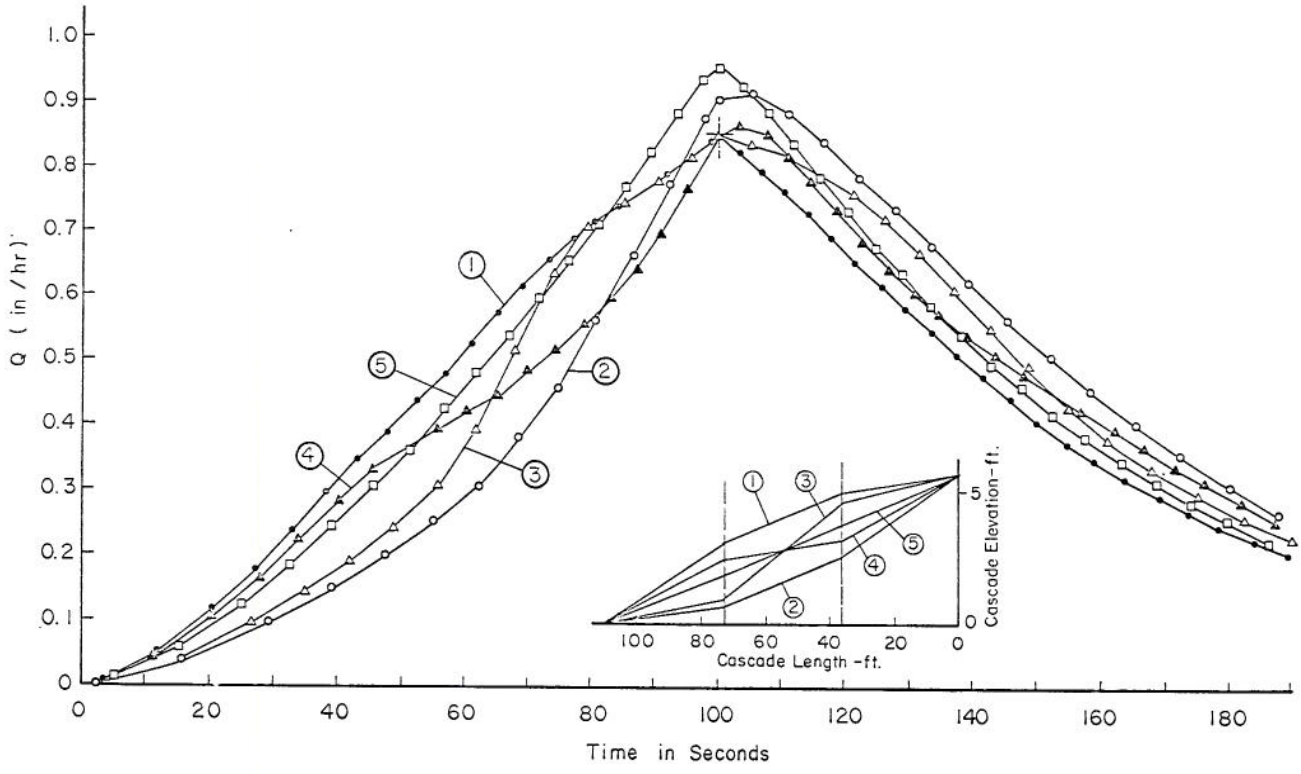

Figure 16. Effect of slope-shape on hydrographs.

Chapter VI

COMPARISON WITH EXPERIMENTAL DATA

Experimental data have been obtained for the case of converging overland flow at the Colorado State University Experimental Rainfall-Runoff Facility (Dickinson, Holland and Smith, 1967). The geometry of the upper basin of the facility is identical to the section of a cone shown in Figure 13. A 120^{o} sector with L_o = 110 ft. and r = 0.0106 was covered with butyl rubber. Lateral inflow was applied through a grid of sprinklers capable of applying water at four intensities: 0.5, 1.04, 2.39, and 4.22 inches per hour. At the lowest intensity, nozzles are located on the corners of 40-foot equilateral triangles. To obtain the higher intensities, additional nozzles are activated. The rainfall pattern is quite uniform, with coefficients of variation from 18% for 0.5 in./hr. to less than 3% for 4.22 inches per hour.

Runoff rates were measured with a 1.5-ft. H flume equipped with a FW-1 stage recorder that has been modified to attain a complete drum revolution in 30 minutes. Time on the analog chart can be read to 5 seconds.

Experimental runs were performed at each of four intensities. Each run consisted of two parts: an equilibrium run to establish the steady-state input rate, and a partial equilibrium run.

The Chezy C was estimated from the equilibrium run data in the following manner. Woolhiser (1969) presented the following dimensionless equations for recession from equilibrium for flow on a converging surface.

$$Q_* = \frac{x_o \left[2 - (1 - r)\, x_o\right]}{(1+r)} \tag{39}$$

$$t'_* = \left(\frac{1+r}{r}\right)^{\frac{N-1}{N}} \frac{\left\{\left[1-(1-r)x_o\right]^{\frac{2N-1}{N}} - (r)^{\frac{2N-1}{N}}\right\}}{(2N-1)\,(1-r)\left\{x_o\left[2-(1-r)\,x_o\right]\right\}^{\frac{N-1}{N}}} \tag{40}$$

Where Q_* is the dimensionless discharge, r is the convergence parameter, x_o is the origin of the characteristic, t'_* is the time after lateral inflow stops until a characteristic originating at x_o, t_o intersects the downstream boundary $x = 1$, and N is the exponent as defined in equation (3). The dimensionless recession hydrograph can be obtained by substituting values of x_o $(0<x_o<1)$ into equations (39) and (40). This hydrograph is shown in Figure 17.

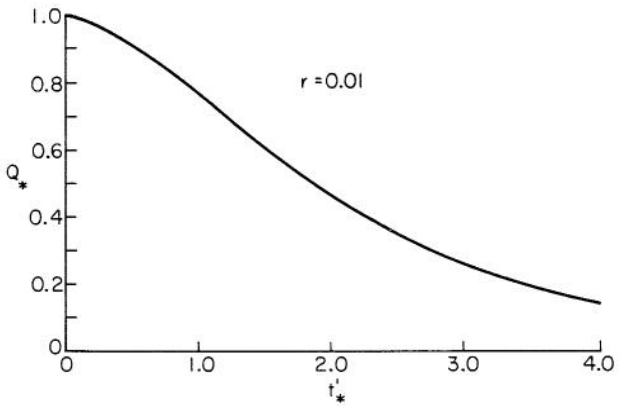

Figure 17. Dimensionless recession hydrograph.

If we assume that the kinematic model with a constant C is adequate for the converging section, we can estimate the normalizing time T_o from the experimental recession from equilibrium and the dimensionless recession curve. On Figure 17 $t'_* = 1$ when $Q_* = 0.76$, $t'_* = 2$ when $Q_* = 0.46$ and $t'_* = 3$ when $Q_* = 0.26$. Let the time after lateral inflow is stopped until the appropriate dimensionless outflow is reached be t_{Q_*}. Then an estimate of T_o is given by

$$T_o = \frac{1}{3}\left[t_{.76} + \frac{1}{2}\,(t_{0.46}) + \frac{1}{3}\,(t_{0.26})\right] \tag{41}$$

Now T_o is defined as the time required to traverse the distance $L_o(1-r)$ at a velocity of V_o where V_o is the normal steady state velocity at the downstream boundary. From equation (3)

$$V_o = \alpha^{1/N}\, Q_o^{\frac{N-1}{N}} = \frac{L_o(1-r)}{T_o} \tag{42}$$

Recalling that $\alpha = C\sqrt{S}$ for the Chézy formulation and $N = 3/2$ we obtain

$$C = \left[\frac{L_o(1-r)}{T_o}\right]^{3/2} \frac{1}{\sqrt{S}\; Q_o} \tag{43}$$

The converging section was approximated with a five-plane cascade with dimensions as shown in Figure 18. The Lax-Wendroff method was used in the numerical calculations and five partial equilibrium cases were simulated. The characteristic method was also used for comparison. Results of the simulations for two partial equilibrium runs are shown in Figure 19 (a) and (b). In both cases the computed peak rates were higher than the observed peaks, but this was not the general case. In two of the five cases simulated, computed peak rates were less than the observed rate. In general, the observed hydrographs rise more slowly during the initial stages than do the computed hydrographs. Although analysis has not proceeded far enough to explain this discrepancy, it could be accounted for by any one or a combination of the following:

(1) Flow is initially laminar

(2) A stilling-well lag

(3) Interception losses occur so that only part of the area contributes initially.

The timing of the peaks agrees very well and the recession hydrograph is accurately simulated by the kinematic cascade.

Additional analyses of experimental data will be required before definitive conclusions can be reached but it appears that the kinematic cascade adequately simulates linearly converging overland flow over a butyl surface. By induction we might assume that the cascade could simulate more complicated converging flow situations.

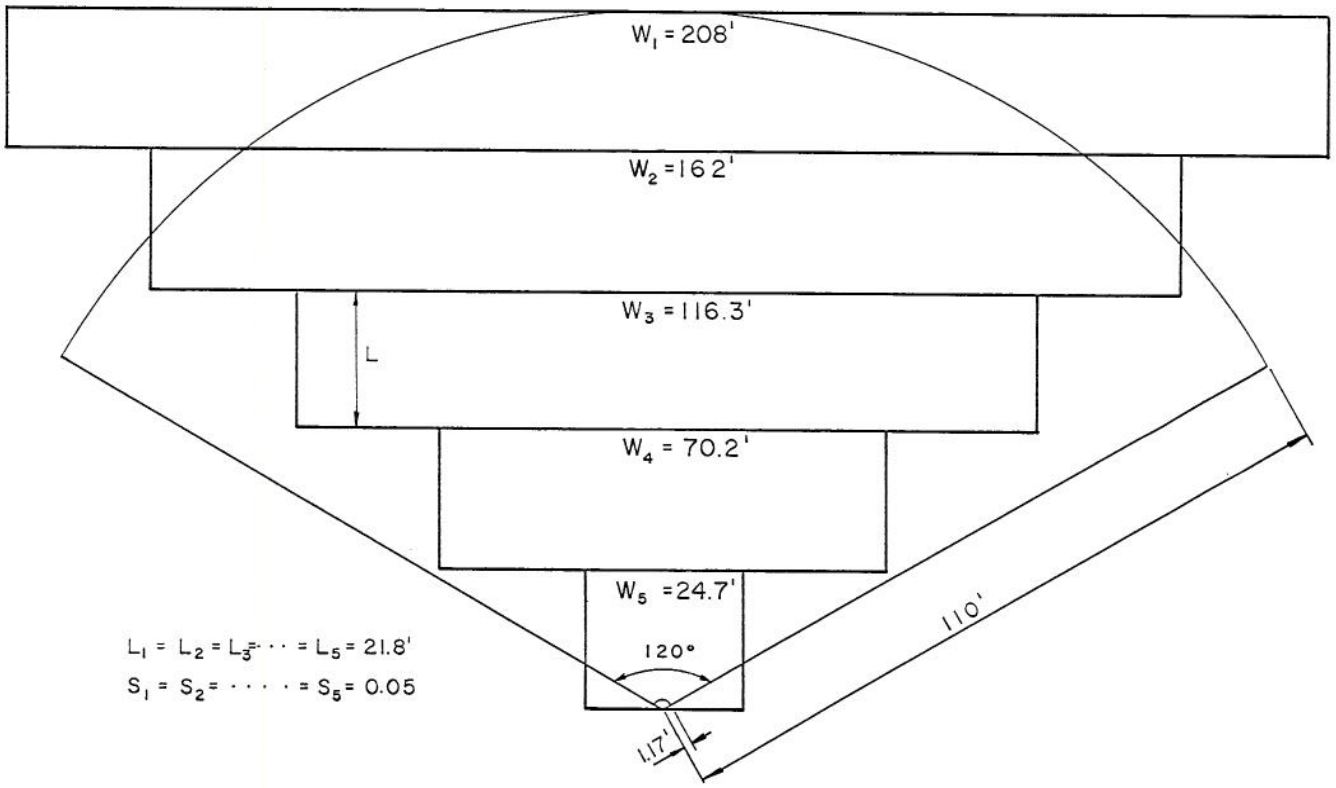

Figure 18. Cascade approximation of converging section.

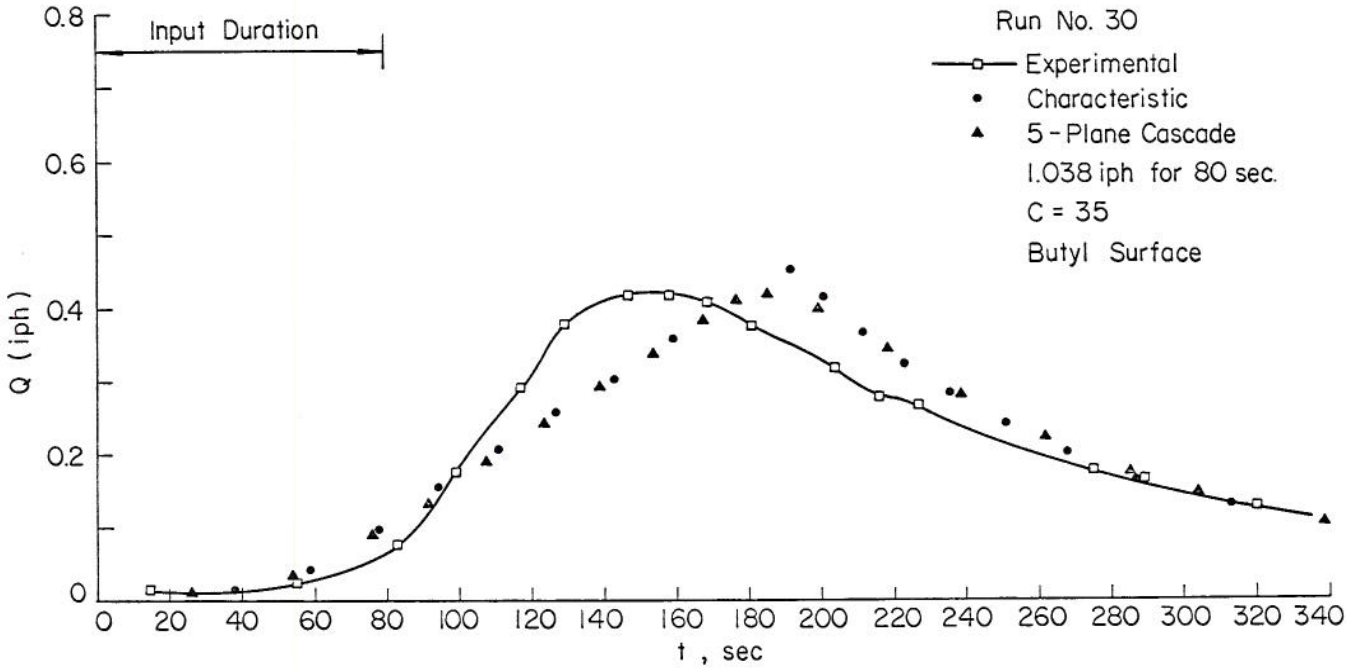

(a)

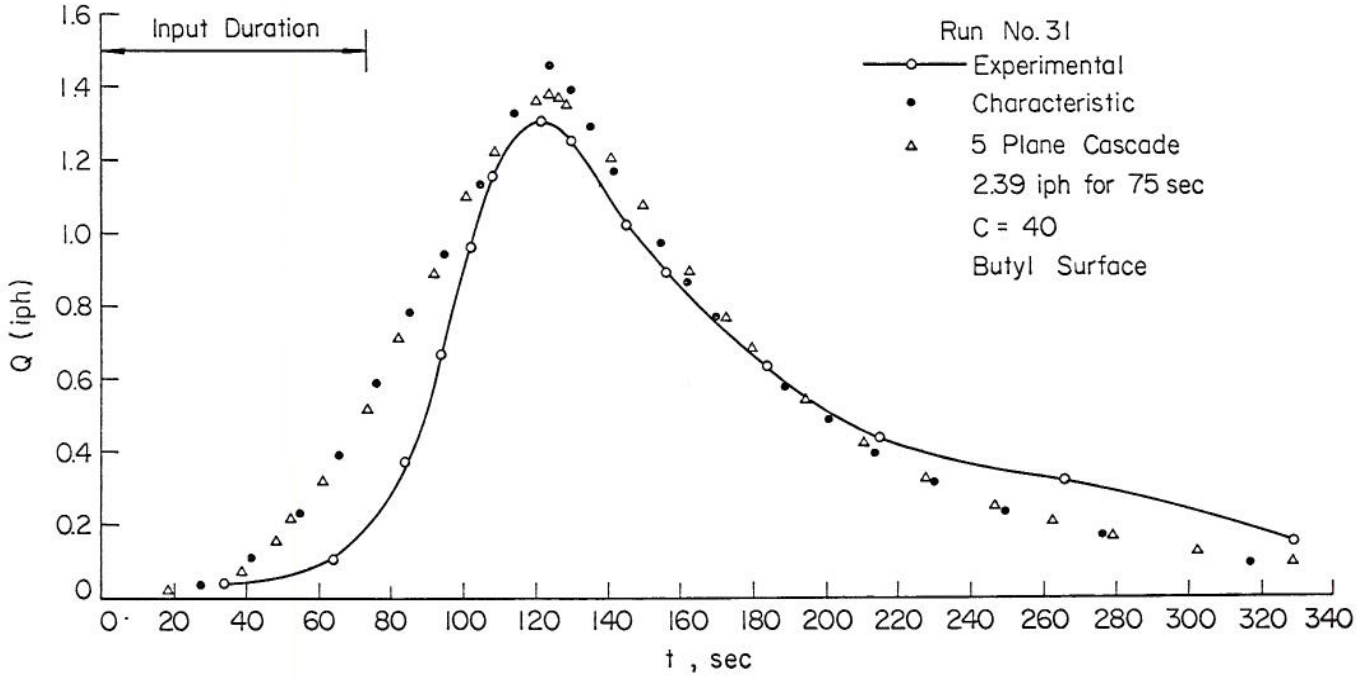

(b)

Figure 19. Comparison of kinematic cascade results with experimental data.

Chapter VII

SUMMARY AND CONCLUSIONS

It was hypothesized that the kinematic cascade is an appropriate mathematical model for describing the dynamic behavior of surface runoff. The mathematical properties of the kinematic cascade were first investigated. Solutions obtained by the method of characteristics were used as standards of comparison in examining other finite-difference schemes. The application of the kinematic cascade to complex watersheds was investigated by comparing cascade solutions to exact solutions and to experimental observations for flow on a linearly converging surface.

The following conclusions may be drawn from this study.

Mathematical Properties of Kinematic Cascade

From the results obtained for both full and partial equilibrium flow conditions, it is evident that the abrupt increase in discharge produced by the shock can be severe, particularly for high P_s values. The results of the 2-plane cascade tests demonstrate that the velocity of the shock, and therefore its path in the x-t plane, is dependent on the parameters P_s and α_2 which are computed from the physical specification for a given plane in the cascade. The shock-parameter, P_s, has been shown to be most closely related to the strength of the shock and therefore influences its celerity or relative velocity. The slope-parameter, α_2, on the other hand, governs the velocity of the flow immediately downstream of the shock. Hence, the absolute propagation speed of the kinematic shock is related to the two interdependent parameters, α_2 and P_s.

While the shock-wave phenomenon may arise under certain highly selective physical circumstances, it is looked upon in this study as a property of the mathematical equations used to explore the overland flow problem rather than as an observable feature of this hydrodynamic process. Nevertheless, the tendencies toward shock formation inherent in the kinematic wave approximation to the shallow-water equations have been ignored in recent investigations using this approach.

Solutions of the kinematic equations in the presence of shocks were obtained by three rectangular difference schemes to evaluate errors of approximation attributable to various finite-difference methods. The three methods studied were the upstream-differencing method, the single-step Lax-Wendroff scheme, and the four-point implicit scheme used by Brakensiek. Of these three methods, the Lax-Wendroff scheme yielded the best approximation to the exact solution obtained by the method of characteristics. The smoothing effect of all rectangular methods in the shock-affected region of the hydrograph was clearly visible and, in general, the hydrograph peak was reduced and delayed by as much as 20 percent for the first-order schemes. The significance of these errors requires further study.

Applications of the Kinematic Cascade to Complex Watersheds

In order to investigate the lumped errors associated with both the finite-difference scheme and the kinematic transformation of a watershed surface, kinematic cascade hydrographs were compared with the exact solutions obtained for flow on a linearly converging surface. Results of this application indicate that the kinematic cascade effectively reduces geometric complexity and accurately simulates overland flow derived from rather complex watershed surfaces. Investigation of the effects of changing overland slope on the outflow from the kinematic cascade revealed a strong correlation between the general shape of the rising hydrograph and the profile of overland slope for the cascade.

Although additional analysis of experimental data will be required before definitive conclusions can be reached, it appears that the kinematic cascade accurately simulates linearly converging flow on an impervious butyl surface.

BIBLIOGRAPHY

1. Brakensiek, D. L., Hydrodynamics of Overland Flow and Nonprismatic Channels. Trans. ASAE, Vol. 9, No. 1, pp. 119-122, 1966.

2. Brakensiek, D. L., A Simulated Watershed Flow System for Hydrograph Prediction: A Kinematic Application. Paper No. 3, Proc. of the Int'l Hydrology Symposium, Fort Collins, Colorado, 1967a

3. Brakensiek, D. L., Kinematic Flood Routing. Trans. ASAE, Vol. 10, No. 3, pp. 340-343, 1967b.

4. Dickinson, W. T., Holland, M. E., and Smith, G. L., An Experimental Rainfall-Runoff Facility. Hydrology Paper No. 25, Colorado State University, Fort Collins, Colorado, 81 pp., 1967.

5. Henderson, F. M., Flood Waves in Prismatic Channels. Jour. Hydraulics Div. Amer. Soc. Civ. Engineers, Hy. 4, 1963.

6. Henderson, F. M., and Wooding, R. A., Overland Flow and Groundwater Flow from a Steady Rainfall of Finite Duration. Jour. Geophysical Research, Vol. 69, No. 8, pp. 1531-1540, 1964.

7. Houghton, David D., and Kasahara, Akira, Nonlinear Shallow Fluid Flow Over an Isolated Ridge. Communication on Pure and Applied Mathematics, Vol. XXI, 1968.

8. Huggins, L. F., and Monke, E. J., A Mathematical Model for Simulating the Hydrologic Response of a Watershed. Paper presented at December 1966 meeting of ASAE, Chicago, Illinois.

9. Iwagaki, Y., Fundamental Studies on Runoff Analysis by Characteristics. Disaster Prevention Research Institute Bulletin No. 10, Kyoto University, Kyoto, Japan, 1955.

10. Izzard, C. F., Hydraulics of Runoff from Developed Surfaces. Proc. Highway Research Board, Vol. 26, pp. 129-146, 1946.

11. Kibler, D. F., A Kinematic Overland Flow Model and its Optimization. Ph.D. Thesis, Colorado State University, Fort Collins, 1968.

12. Liggett, J. A., General Solution for Open Channel Profiles, Proc. ASCE, HY 6, November 1961.

13. Lighthill, M. J., and Whitham, C. B., On Kinematic Waves. I. Flood Movement in Long Rivers. Proc. of the Royal Society of London, Series A, Vol. 229, 1955.

14. Morgali, J. R., Laminar and Turbulent Overland Flow. Paper presented at the 49th Annual Meeting American Geophysical Union, Washington, D. C., 1968.

15. Veal, D. G., A Computer Solution of Converging, Subcritical Overland Flow. M.S. Thesis, Cornell University, 1966.

16. Wooding, R. A., A Hydraulic Model for the Catchment-stream Problem. (a) I. Kinematic Wave Theory. (b) II. Numerical Solutions. (c) III. Comparison with Runoff Observations. Jour. of Hydrology, Vol. 3, 1965.

17. Woolhiser, D. A., Overland Flow on a Converging Surface. Trans. ASAE, Vol. 12, No. 4, pp. 460-462, 1969.

18. Woolhiser, D. A., and Liggett, J. A., Unsteady, One-dimensional Flow over a Plane--the Rising Hydrograph. Water Resources Research, Vol. 3, No. 3, pp. 753-771, 1967.

APPENDIX A

Derivation of the Shallow-water Equations

Introduction

The flow of surface water over a uniform plane or in a channel is classified as spatially varied and unsteady. Accordingly, the basic equations of the kinematic model designed to simulate the surface runoff process are derived from the principles of conservation of mass and momentum. The derivations presented in this section follow the development in standard hydraulic references treating spatially varied unsteady flow. The dependent quantities are the local velocity, u, in fps and depth, h, in feet. The independent variables are the space-time coordinates, x in feet and t in seconds, respectively.

Continuity Equation

The sketch of Figure A.1 illustrates the variables used in deriving the continuity equation for a plane or channel element of arbitrary cross-section having one-dimensional flow. The continuity equation written over a time increment dt for the element of fluid shown in Figure A.1 is:

$$(A.u + q.dx)\,dt - (A + \frac{\partial A}{\partial x}\,dx)\,(u + \frac{\partial u}{\partial x}\,dx)\,dt =$$

(inflow) (outflow)

$$\frac{\partial A}{\partial t}\,dt.dx \qquad \text{(A-1)}$$

(change in storage)

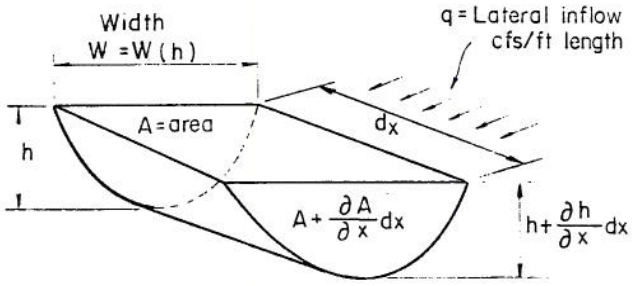

Figure A.1 Definition sketch for continuity equation.

Cancelling the product $A \cdot u$, dividing by $dx \cdot dt$, and neglecting the higher order products, equation (A-1) becomes:

$$\frac{\partial A}{\partial t} + A\frac{\partial u}{\partial x} + u\frac{\partial A}{\partial x} = q \qquad \text{(A-2)}$$

For channels of triangular or rectangular cross-section, the area can be expressed in the form:

$$A = bh^m \qquad \text{(A-3)}$$

The constants b and m are equal to the width, W, and 1, respectively, for a rectangular section, and equal to the side slope, Z, and 2, respectively, for a triangular section. Substitution of (A-3) in equation (A-2) yields the following relation:

$$b \cdot m \cdot h^{m-1}\frac{\partial h}{\partial t} + b \cdot h^m \frac{\partial u}{\partial x} + b \cdot m \cdot h^{m-1} u\frac{\partial h}{\partial x} = q \qquad \text{(A-4)}$$

In the case of a wide plane or channel, equation (A-4) can be written as:

$$\frac{\partial h}{\partial t} + u\frac{\partial h}{\partial x} + h\frac{\partial u}{\partial x} = q \qquad \text{(A-5)}$$

Equation (A-5) is the one-dimensional continuity equation for surface flow over a wide plane or channel.

Momentum Equation

An element of fluid receiving lateral inflow in cfs/sq.ft. is shown in Figure A.2. Newton's second

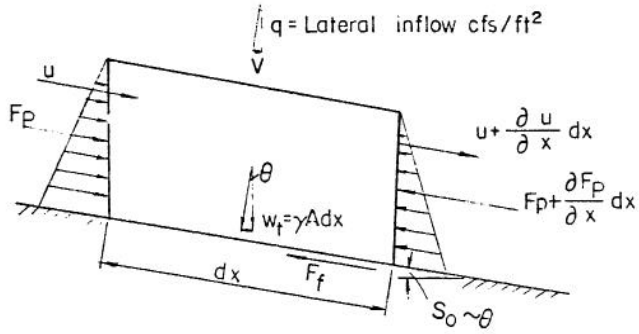

Figure A.2 Forces acting on fluid element used in deriving the momentum equation.

law is written for the forces acting in the x-direction, where x is measured downstream. The lateral inflow has a velocity component, v, in the x-direction. The basic equation to be satisfied is:

$$\Sigma F_x = m_s \frac{du}{dt} + m_l \frac{dv}{dt} \qquad \text{(A-6)}$$

where m_s and m_l are the masses of water in the main stream and lateral inflow, respectively.

Forces acting in the x-direction on the element are the following:

(1) The weight component acting in the downstream direction.

$$W_t \cdot \sin\theta = \gamma A \sin\theta \, dx \approx \gamma A \, S_o \, dx$$

where γ is the unit weight of water and S_o the bed slope;

(2) The hydrostatic force acting to the right of the centroid of area

$$F = \gamma \bar{h} A,$$

where $\bar{h}$ is the distance from the water surface to the centroid of area A;

(3) The hydrostatic force acting to the left at the centroid of area

$$F_p + \frac{\partial F_p}{\partial x} dx = \gamma \bar{h} A + \frac{\partial F_p}{\partial x} dx$$

Liggett (1961) has shown that the hydrostatic pressure differential, $\frac{\partial F_p}{\partial x} dx$, is given by

$$\frac{\partial F_p}{\partial x} dx = -\gamma A \frac{\partial h}{\partial x} dx; \text{ and}$$

(4) The friction force retarding the flow

$$F_f = -\gamma A \, S_f \, dx$$

where S_f is the slope of the energy line.

Hence the basic equation (A-6) may be written as

$$\Sigma F_x = \gamma A \, S_o \, dx - \gamma A \, S_f \, dx - \gamma A \frac{\partial h}{\partial x} dx \qquad (A\text{-}7)$$

The momentum changes on the RHS of equation (A-6) may be evaluated as

$$m_s \frac{du}{dt} = \frac{1}{g} \gamma A dx \frac{du}{dt}$$

$$= \frac{1}{g} \gamma A \, dx \left(\frac{\partial u}{\partial t} + \frac{\partial u}{\partial x} \cdot \frac{dx}{dt}\right)$$

$$= \frac{1}{g} \gamma A \, dx \left(\frac{\partial u}{\partial t} + u \frac{\partial u}{\partial x}\right) \qquad (A\text{-}8)$$

$$m_l \frac{dv}{dt} = \frac{1}{g} \gamma q \, dx \, dt \, \frac{(u-v)}{dt}$$

$$= \frac{1}{g} \gamma \, q \, (u-v) \, dx \qquad (A\text{-}9)$$

where g is acceleration due to gravity and $\frac{du}{dt}$ is interpreted as the total derivative of a particle along its stream path.

Combining equations (A-6), (A-7), (A-8) and (A-9) yields the momentum expression:

$$\gamma A \, S_o \, dx - \gamma A \, S_f \, dx - \gamma A \frac{\partial h}{\partial x} dx = \frac{1}{g} \gamma A \, dx \left(\frac{\partial u}{\partial t} + u \frac{\partial u}{\partial x}\right)$$

$$+ \frac{1}{g} \gamma q \, (u-v) \, dx \qquad (A\text{-}10)$$

Dividing (A-10) by $\frac{1}{g} \gamma A \, dx$ and re-arranging:

$$\frac{\partial u}{\partial t} + u \frac{\partial u}{\partial x} + g \frac{\partial h}{\partial x} = g(S_o - S_f) - \frac{q}{A}(u-v) \qquad (A\text{-}11)$$

For the case of one-dimensional flow in a wide channel or over a plane surface, equation (A-11) can be written:

$$\frac{\partial u}{\partial t} + u \frac{\partial u}{\partial x} + g \frac{\partial h}{\partial x} = g(S_o - S_f) - \frac{q}{h}(u-v) \qquad (A\text{-}12)$$

Equations (A-5) and (A-12) are the one-dimensional unsteady spatially varied flow equations applicable to wide channels and overland flow planes. The assumptions made during their derivation are the following:

(1) The flow is gradually varied so that vertical components of velocity and acceleration are negligible in comparison with the components along the direction of flow.

(2) The pressure on the vertical surfaces of the flow element is hydrostatic.

(3) The energy and momentum coefficients, used as corrections to nonuniform velocity distributions, are equal to one.

(4) The channel slope, S_o, is small and is approximately equal to $\sin\theta \approx \theta$.

(5) Frictional resistance in unsteady flow is the same as that for the corresponding depth in uniform flow so that the friction slope, S_f, can be obtained by either the Manning or Chézy friction relations.

Reference is made to publications by Gilcrest (1950), Chow (1959) and Yevjevich (1961) for more extensive treatment of the spatially varied unsteady flow equations.

APPENDIX B

Derivation of Lax-Wendroff Scheme

The dimensionless equation for kinematic flow is

$$\frac{\partial h}{\partial t} + \beta h^{N-1} \frac{\partial h}{\partial x} = q \qquad \text{(B-1)}$$

where $\beta = Nk/n$

This equation can be written in the conservation form:

$$\frac{\partial h}{\partial t} + \frac{\partial}{\partial x}\left(\frac{k}{n} h^N\right) - q = 0 \qquad \text{(B-2)}$$

Expanding $h(x,t+\Delta t)$ in a Taylors Series we obtain:

$$h(x,t+\Delta t) = h(x,t) + \Delta t \frac{\partial h}{\partial t} + \frac{\Delta t^2}{2} \frac{\partial^2 h}{\partial t^2} + 0(\Delta t)^3 \qquad \text{(B-3)}$$

From equation (B-2)

$$\frac{\partial h}{\partial t} = -\left[\frac{\partial}{\partial x}\left(\frac{k}{n} h^N\right) - q\right] \qquad \text{(B-4)}$$

and

$$\frac{\partial^2 h}{\partial t^2} = \frac{\partial}{\partial t} - \left[\frac{\partial}{\partial x}\left(\frac{k}{n} h^N\right) - q\right] = -\frac{\partial}{\partial x}\left[\frac{\partial}{\partial t}\frac{k}{n} h^N\right] + \frac{\partial q}{\partial t}$$

$$= -\frac{\partial}{\partial x}\left[N \frac{k}{n} h^{N-1} \frac{\partial h}{\partial t}\right] + \frac{\partial q}{\partial t} \qquad \text{(B-5)}$$

Substituting the expression for $\frac{\partial h}{\partial t}$ given by equation (B-4) into equation (B-5)

$$\frac{\partial^2 h}{\partial t^2} = \frac{\partial}{\partial x}\left[N \frac{k}{n} h^{N-1}\left(\frac{\partial}{\partial x}\left(\frac{k}{n} h^N\right) - q\right)\right] + \frac{\partial q}{\partial t} \qquad \text{(B-6)}$$

Therefore:

$$h(x,t+\Delta t) = h(x,t) - \Delta t\left[\frac{\partial}{\partial x}\left(\frac{k}{n} h^N\right) - q\right]$$

$$+ \frac{\Delta t^2}{2}\left\{\frac{\partial}{\partial x}\left[\frac{Nkh^{N-1}}{n}\left(\frac{\partial}{\partial x}\left(\frac{k}{n} h^N\right) - q\right)\right] + \frac{\partial q}{\partial t}\right\} \qquad \text{(B-7)}$$

Equation (B-7) gives a second order approximation for $h(x,t+\Delta t)$ and is the basis of the finite-difference formulation shown in Table 3.

APPENDIX C

Stability Calculations

Stability is one of the properties of a difference scheme that is required before convergence is guaranteed. In an unstable scheme small numerical errors introduced in the computational method are amplified and eventually dominate the solution. Although the following method of stability analysis is not rigorous for nonlinear equations, it does serve to identify those difference schemes that are obviously unsuitable and it also determines appropriate step lengths for conditionally stable schemes.

In a linear stability analysis we assume that instabilities first appear in a very small region of space so that if the coefficients of the derivatives are smooth functions they can be approximated as constants in this region. Accordingly, we linearize equation (11) as shown in equation (C-1) where $\bar{h}$ is a constant.

$$\frac{\partial h}{\partial t} + \beta \bar{h}^{N-1} \frac{\partial h}{\partial x} = q \qquad \text{(C-1)}$$

Now at any point j, k the numerical solution h_j^k is equal to the true solution $h(k\Delta t, j\Delta x)$ plus an error term $\tilde{h}_j^k$.

$$h_j^k = h(k\Delta t, j\Delta x) + \tilde{h}_j^k \qquad \text{(C-2)}$$

where Δt is the time increment and Δx is the distance increment.

Because we are dealing with a linear system, we can consider one term of the Fourier Series expression for the error term.

$$\tilde{h}_m^n = H_0 \exp\left[i(m\sigma\Delta x + n\gamma\Delta t)\right] \qquad \text{(C-3)}$$

where H_0 is a constant, σ and γ are wave numbers in space and time and $i = \sqrt{-1}$. It is assumed that the errors are perturbations added to the solution of the linear system. If we write the linearized finite-difference equation in terms of the correct solution plus the error terms (equation (C-2)) and then subtract the exact equation, we can obtain a differential equation in the error terms. This differential equation is then written in finite-difference form. In a stable scheme the ratio of successive error terms will be smaller than unity, e.g.,

$$\left| \frac{\tilde{h}_j^{k+1}}{\tilde{h}_j^{k}} \right| \leq 1 \qquad \text{(C-4)}$$

which establishes a stability criterion.

Lax-Wendroff Method

The linearized Lax-Wendroff scheme in the error terms is

$$\tilde{h}_j^{k+1} = \tilde{h}_j^{k} - \Delta t \left[a \left(\frac{\tilde{h}_{j+1}^{k} - \tilde{h}_{j-1}^{k}}{2\Delta x} \right) \right]$$

$$+ \frac{\Delta t^2}{2} \left\{ \frac{a^2}{\Delta x^2} \left(\tilde{h}_{j+1}^{k} - 2\tilde{h}_j^{k} + \tilde{h}_{j-1}^{k} \right) \right\} \qquad \text{(C-5)}$$

where: $a = \frac{N k \bar{h}^{N-1}}{n}$

If in equation (C-3) we let $m = n = 0$ for point j, k (which we can do with no loss in generality) we obtain the following

$$\tilde{h}_j^{k} = H_o \; ; \; \tilde{h}_j^{k+1} = H_o \exp\left[i\gamma\Delta t\right]$$

$$\tilde{h}_{j+1}^{k} = H_o \exp\left[i\sigma\Delta x\right] \; ; \; \tilde{h}_{j-1}^{k} = H_o \exp\left[-i\sigma\Delta x\right]$$

Substituting these expressions into equation (C-5) and dividing by $\tilde{h}_j^k$

$$\tilde{h}_j^{k+1} / \tilde{h}_j^{k} = e^{i\gamma\Delta t} = 1 - \frac{a\Delta t}{2\Delta x}\left[e^{i\sigma\Delta x} - e^{-i\sigma\Delta x}\right]$$

$$+ \frac{1}{2}\left(\frac{\Delta t}{\Delta x} a\right)^2 \left[e^{i\sigma\Delta x} - 2 + e^{-i\sigma\Delta x}\right] \qquad \text{(C-6)}$$

with the appropriate trignometric substitutions

$$e^{i\gamma\Delta t} = 1 + a\frac{\Delta t}{\Delta x}(i \sin \sigma\Delta x) + \left(\frac{\Delta t}{\Delta x} a\right)^2 (\cos \sigma\Delta x - 1) \qquad \text{(C-7)}$$

For stability, the quantity $e^{i\gamma\Delta t}$ must lie within the unit circle on the complex plane. Now the real part of equation (C-7) is

$$1 + \left(a\frac{\Delta t}{\Delta x}\right)^2 (\cos \sigma\Delta x - 1)$$

and the imaginary part is

$$a\frac{\Delta t}{\Delta x}\sin\sigma\Delta x \quad .$$

Squaring the real and imaginary parts we obtain the criterion

$$\left| 1 + r^2\left[2(\cos\theta-1) + r^2(\cos^2\theta-2\cos\theta+1) + \sin^2\theta\right]\right| \le 1 \qquad \text{(C-8)}$$

where $r = \theta\Delta t/\Delta x$ and $\theta = \sigma\Delta x$

Let us consider the most critical condition when the left-hand side of equation (C-8) is evaluated at the following values of $\sigma\Delta x$

$\sigma\Delta x$	$\sin\sigma\Delta x$	$\cos\sigma\Delta x$	Criterion
0	0	1	$\left\|1\right\| \le 1$
$\pi/2$	1	0	$\left\|1-(a\frac{\Delta t}{\Delta x})^2 + (\frac{a\Delta t}{\Delta x})^4\right\| \le 1$
π	0	-1	$\left\|1-4(a\frac{\Delta t}{\Delta x})^2 + 4(\frac{a\Delta t}{\Delta x})^4\right\| \le 1$
$3\pi/2$	-1	0	$\left\|1-(a\frac{\Delta t}{\Delta x})^2 + (\frac{a\Delta t}{\Delta x})^4\right\| \le 1$

From the analysis, it is clear that the criterion stated above is satisfied when

$$(a\frac{\Delta t}{\Delta x})^2 \le 1$$

$$a\frac{\Delta t}{\Delta x} \le 1$$

or

$$\frac{\Delta t}{\Delta x} \le \frac{n}{N\bar{k}\bar{h}^{N-1}} \qquad \text{(C-9)}$$

Equation (C-9) shows that the point $k+1$, j must lie within the zone of determinacy of the line from k, $j-1$ to k, $j+1$. The Lax-Wendroff scheme is linearly stable subject to condition (C-9).

Upstream differencing method

When the upstream differencing method (Table 3) is applied to the linearized equation with the error terms and the exact equations are subtracted we obtain:

$$\tilde{h}_j^{k+1} = \tilde{h}_j^k - a\frac{\Delta t}{\Delta x}(\tilde{h}_j^k - \tilde{h}_{j-1}^k) \qquad \text{(C-10)}$$

where: $a = \frac{N\bar{k}\bar{h}^{N-1}}{n}$

After substituting the Fourier expressions for the error terms

$$e^{i\gamma\Delta t} = 1 - a\frac{\Delta t}{\Delta x}(1 - e^{-i\sigma\Delta x}) \qquad \text{(C-11)}$$

For the stability we require

$$\left|1 - a\frac{\Delta t}{\Delta x}(1 - e^{-i\sigma\Delta x})\right| \le 1$$

or $$\left|1 - a\frac{\Delta t}{\Delta x}(1 - \cos\sigma\Delta x + i\sin\sigma\Delta x)\right| \le 1 \quad .$$

Squaring the real and imaginary parts,

$$\left|1 - 2a\frac{\Delta t}{\Delta x}\left[a\frac{\Delta t}{\Delta x}(1 - \cos\sigma\Delta x) + (1 - \cos\sigma\Delta x)\right]\right| \le 1 \qquad \text{(C-12)}$$

Upon simplification, inequality (C-12) becomes

$$a\frac{\Delta t}{\Delta x} \le -\frac{1+\sqrt{3}}{2}$$

or

$$\frac{\Delta t}{\Delta x} \le \frac{n}{2.75Nk\bar{h}^{N-1}} \qquad \text{(C-13)}$$

Brakensiek's four-point implicit method

Using the same procedures outlined above, the stability criterion for the implicit method is:

$$\left|\frac{\frac{\Delta t}{\Delta x}(\cos\theta - i\sin\theta + 1)}{\left(1 - \frac{\Delta t}{\Delta x}\right)(\cos\theta - i\sin\theta) - \left(1 + \frac{\Delta t}{\Delta x}\right)}\right| \le 1$$

which can be put in the form

$$\left|\frac{\sqrt{2\left(\frac{\Delta t}{\Delta x}\right)^2\left[1+\cos\theta\right]}\, e^{i\theta_1}}{\sqrt{2\left(\frac{\Delta t}{\Delta x}\right)^2\left[1+\cos\theta\right] + 2(1-\cos\theta)}\, e^{i\theta_2}}\right| \le 1 \qquad \text{(C-14)}$$

where $\theta = \sigma\Delta t$.

The left-hand side of inequality (C-14) is always ≤ 1 so the scheme is unconditionally stable.

Key Words: Overland flow, Open channel flow, Kinematic, Numerical Methods, Watershed models

Abstract: A kinematic cascade is defined as a sequence of n discrete overland flow planes or channel segments in which the kinematic wave equations are used to describe the unsteady flow. Each plane or channel is characterized by a length, l_k, width, w_k, and a roughness-slope factor, α_k. Outflow from the k^{th} plane, along with the parameters for planes k and $k + 1$, establishes the upstream boundary condition for plane $k + 1$. Nondimensional equations are presented for the k^{th} element in a kinematic cascade. Properties of the solutions for a kinematic cascade with pulsed lateral inputs are examined. Cascade solutions are compared with characteristic-analytic solutions and with experimental data for flow over a linearly converging section.

References: David F. Kibler and David A. Woolhiser, Colorado State University Hydrology Paper No. 39 (March 1970) "The Kinematic Cascade as a Hydrologic Model."

Key Words: Overland flow, Open channel flow, Kinematic, Numerical Methods, Watershed models

Abstract: A kinematic cascade is defined as a sequence of n discrete overland flow planes or channel segments in which the kinematic wave equations are used to describe the unsteady flow. Each plane or channel is characterized by a length, l_k, width, w_k, and a roughness-slope factor, α_k. Outflow from the k^{th} plane, along with the parameters for planes k and $k + 1$, establishes the upstream boundary condition for plane $k + 1$. Nondimensional equations are presented for the k^{th} element in a kinematic cascade. Properties of the solutions for a kinematic cascade with pulsed lateral inputs are examined. Cascade solutions are compared with characteristic-analytic solutions and with experimental data for flow over a linearly converging section.

References: David F. Kibler and David A. Woolhiser, Colorado State University Hydrology Paper No. 39 (March 1970) "The Kinematic Cascade as a Hydrologic Model."

Key Words: Overland flow, Open channel flow, Kinematic, Numerical Methods, Watershed models

Abstract: A kinematic cascade is defined as a sequence of n discrete overland flow planes or channel segments in which the kinematic wave equations are used to describe the unsteady flow. Each plane or channel is characterized by a length, l_k, width, w_k, and a roughness-slope factor, α_k. Outflow from the k^{th} plane, along with the parameters for planes k and $k + 1$, establishes the upstream boundary condition for plane $k + 1$. Nondimensional equations are presented for the k^{th} element in a kinematic cascade. Properties of the solutions for a kinematic cascade with pulsed lateral inputs are examined. Cascade solutions are compared with characteristic-analytic solutions and with experimental data for flow over a linearly converging section.

References: David F. Kibler and David A. Woolhiser, Colorado State University Hydrology Paper No. 39 (March 1970) "The Kinematic Cascade as a Hydrologic Model."

Key Words: Overland flow, Open channel flow, Kinematic, Numerical Methods, Watershed models

Abstract: A kinematic cascade is defined as a sequence of n discrete overland flow planes or channel segments in which the kinematic wave equations are used to describe the unsteady flow. Each plane or channel is characterized by a length, l_k, width, w_k, and a roughness-slope factor, α_k. Outflow from the k^{th} plane, along with the parameters for planes k and $k + 1$, establishes the upstream boundary condition for plane $k + 1$. Nondimensional equations are presented for the k^{th} element in a kinematic cascade. Properties of the solutions for a kinematic cascade with pulsed lateral inputs are examined. Cascade solutions are compared with characteristic-analytic solutions and with experimental data for flow over a linearly converging section.

References: David F. Kibler and David A. Woolhiser, Colorado State University Hydrology Paper No. 39 (March 1970) "The Kinematic Cascade as a Hydrologic Model."